

Versatility of the Curcumin Scaffold: Discovery of Potent and Balanced Dual BACE-1 and GSK-3 $\beta$  Inhibitors

Rita Maria Concetta Di Martino,<sup>†</sup> Angela De Simone,<sup>‡</sup> Vincenza Andrisano,<sup>‡</sup> Paola Bisignano,<sup>§</sup> Alessandra Bisi,<sup>†</sup> Silvia Gobbi,<sup>†</sup> Angela Rampa,<sup>†</sup> Romana Fato,<sup>†</sup> Christian Bergamini,<sup>†</sup> Daniel I. Perez,<sup>||</sup> Ana Martinez,<sup>||</sup> Giovanni Bottegoni,<sup>§</sup> Andrea Cavalli,<sup>†,§</sup> and Federica Belluti<sup>\*,†</sup>

<sup>†</sup>Department of Pharmacy and Biotechnology, Alma Mater Studiorum - University of Bologna, Via Belmeloro 6, 40126 Bologna, Italy

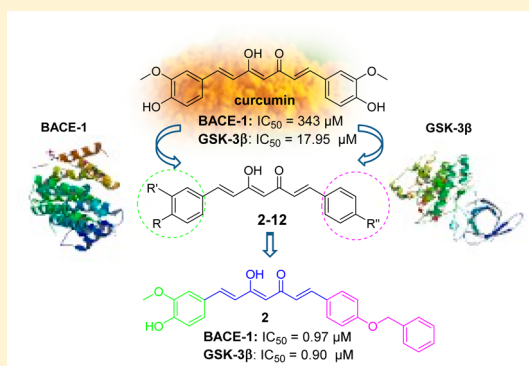
<sup>‡</sup>Department for Life Quality Studies, Alma Mater Studiorum - University of Bologna, Corso D'Augusto 237, 47921 Rimini, Italy

<sup>§</sup>Istituto Italiano di Tecnologia, D3, via Morego 30, 16163 Genova, Italy

<sup>||</sup>Centro de Investigaciones Biologicas, CSIC, Ramiro de Maetzu 9, 28040 Madrid, Spain

**S** Supporting Information

**ABSTRACT:** The multitarget approach has gained increasing acceptance as a useful tool to address complex and multifactorial maladies such as Alzheimer's disease (AD). The concurrent inhibition of the validated AD targets  $\beta$ -secretase (BACE-1) and glycogen synthase kinase-3 $\beta$  (GSK-3 $\beta$ ) by attacking both  $\beta$ -amyloid and tau protein cascades has been identified as a promising AD therapeutic strategy. In our study, curcumin was identified as a lead compound for the simultaneous inhibition of both targets; therefore, synthetic efforts were dedicated to obtaining a small library of novel curcumin-based analogues, and a number of potent and balanced dual-target inhibitors were obtained. In particular, **2**, **6**, and **7** emerged as promising drug candidates endowed with neuroprotective potential and brain permeability. Notably, for some new compounds the symmetrical diketo and the  $\beta$ -keto–enol tautomeric forms were purposely isolated and tested *in vitro*, allowing us to gain insight into the key requirements for BACE-1 and GSK-3 $\beta$  inhibition.



## INTRODUCTION

Alzheimer's disease (AD), the most common form of dementia in industrialized nations among the elderly, is a progressive degenerative disorder, characterized by massive neuronal death and synaptic degeneration, that ultimately leads to the collapse of the neural networks essential for cognition and memory. It is the sixth leading cause of death, currently affecting more than 44 million people worldwide and, due to its debilitating nature, causes enormous financial and emotional stress on patients and caregivers. Considering that worldwide the population is rapidly aging, the number of AD patients is projected to reach 116 million by 2050.<sup>1</sup> The current FDA-approved therapies for moderate to severe AD provide only temporary and incomplete symptomatic relief and only represent a palliative tool to slow down the clinical course of the disease.<sup>2</sup> The lack of truly effective drugs is related to the multifactorial nature of the disease, in which several impaired molecular pathways interact in a feed-forward loop.<sup>3,4</sup>

Aberrant protein processing is a distinctive feature of AD, in which amyloid  $\beta$  (A $\beta$ ) peptide and abnormally hyperphosphorylated tau protein, upon misfolding, self-assemble and accumulate in the brain as aggregates, namely, amyloid senile plaques (SPs) and neurofibrillary tangles (NFTs), respectively.<sup>5</sup> These assemblies represent the most relevant

histopathological hallmarks of the disease and have been considered to play crucial roles in its pathogenesis. Through different molecular mechanisms, these aggregates trigger a cascade of biological processes, among others, amyloid and tau cascades, ultimately culminating in neuronal cell death, brain atrophy, and cognitive decline.

Research programs focused on the amyloid cascade still occupy a relevant place, as documented by the substantial number of compounds entered in clinical trials,<sup>6</sup> together with the large amount of published manuscripts. A $\beta$  peptide is generated through a sequential proteolysis of the amyloid  $\beta$  protein precursor (APP) catalyzed by  $\beta$ - and  $\gamma$ -secretases.<sup>7</sup> In this context, the inhibition of  $\beta$ -secretase, an aspartyl protease also known as  $\beta$ -site APP cleaving enzyme (or BACE-1), regulating the first and rate-limiting step of APP processing, could efficiently block the production of A $\beta$  and of other post-translational products.<sup>8</sup> The higher BACE-1 expression and activity detected in AD patients' brains are consistent with the elevated A $\beta$  levels.<sup>9</sup> The availability of the BACE-1 crystal structure greatly enabled the drug development process in this field. This aspartyl protease is characterized by a bilobal

Received: June 10, 2015

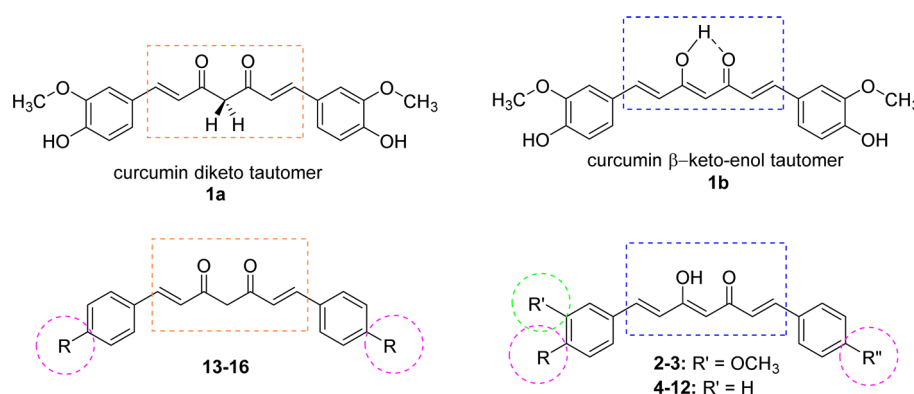


**Figure 1.** Design strategy toward the synthesized curcumin-based analogues (2–16). Structure of the tautomeric forms of curcumin (diketo tautomer **1a** and  $\beta$ -keto-enol tautomer **1b**) and general formula of the synthesized curcumin-based analogues (2–12 and 13–16). For structures, see Tables 1 and 2.

structure, the active site is a long cleft for substrate recognition with a flap region that, descending over the top, pins the substrate nearby two catalytic aspartic residues at the site of bond hydrolysis.<sup>10</sup> Interestingly, a molecular interplay between A $\beta$  and tau in causing synergic toxicity is a recent and intriguing finding, even if the molecular basis of the process still remains to be fully deciphered.<sup>11</sup>

Under normal physiological conditions, tau is associated with microtubules and, preventing their dynamic instability, contributes to morphogenesis of neurons.<sup>12</sup> The strong correlation between tau hyperphosphorylation and AD pathology focuses the attention on tau kinases and, glycogen synthase kinase-3 $\beta$  (GSK-3 $\beta$ ), a multitasking serine/threonine kinase largely expressed in the central nervous system (CNS), proved to play a significant role in regulating tau phosphorylation under both physiological and pathological conditions.<sup>13</sup> In particular, GSK-3 $\beta$  dysregulation is believed to contribute, through a large number of cellular processes, to the etiology of chronic conditions such as diabetes, cancer, and CNS disorders, i.e., schizophrenia and AD.<sup>14</sup> GSK-3 $\beta$  induces tau phosphorylation mainly at Ser199, Ser396, and Ser413 and causes tau disjunction from the microtubules and aggregation as NFT.<sup>15</sup> Over the past decade, the increased interest in GSK-3 $\beta$  led to the discovery of a number of inhibitors, based on chemically different molecular scaffolds acting with different mechanisms of action, such as ATP competition, allosteric modulation, and enzyme irreversible inhibition.<sup>16</sup> The last two approaches allowed one to minimize the undesirable off-target effects. In particular, irreversible inhibition, by selective targeting of a nonconserved cysteine residue (Cys199) in the ATP-binding site, was reported as a promising strategy for obtaining useful pharmacological tools.<sup>17,18</sup> Interestingly, the cross-talk between GSK-3 $\beta$  and A $\beta$  suggested GSK-3 $\beta$  as the molecular link between A $\beta$  and tau. The GSK-3 $\beta$  pathological activation by A $\beta$ , through the prevention of the inhibitory phosphorylation of this kinase, leads to an increment of tau phosphorylation.<sup>19,20</sup> Furthermore, inhibition of this kinase decreases A $\beta$  production and A $\beta$ -induced neurotoxicity by reducing the BACE-1 cleavage of APP.<sup>14</sup>

Disease-modifying therapeutics able to target AD's underlying physiopathology would represent an ideal tool to control both the onset and progression of the neurodegenerative process.<sup>21,22</sup> Recently, it has become evident that the concurrent modulation of several targets involved in this complex disease could represent an ideal strategy for achieving

an effective treatment.<sup>23,24</sup> The idea is to devise multitarget agents that might provide a better efficacy profile, compared with a single-target therapeutic.<sup>25</sup> In this respect, a crucial issue of the multitarget drug discovery is the achievement, in a single chemical entity, of balanced potency toward the selected targets.<sup>26</sup> In this scenario, a multitarget approach, based on the simultaneous inhibition of disease-modifying AD relevant targets BACE-1 and GSK-3 $\beta$ , promises to achieve successful AD treatment.<sup>27</sup> To further corroborate this challenging and still underexplored drug discovery hypothesis and as a continuation of our research studies aimed at the discovery of natural product-inspired compounds as multipotent AD drug candidates,<sup>28,29</sup> we rationally designed a new series of dual BACE-1 and GSK-3 $\beta$  inhibitors based on the curcumin scaffold.

Natural products proved to be an excellent source of lead compounds for drug discovery.<sup>30</sup> These small molecules, synthesized by the plant kingdom, are considered as "privileged structures" because they have evolved in the natural selection process to achieve optimal interactions with a number of biological targets.<sup>31</sup> The polyphenol curcumin (**1a**, Figure 1), the primary bioactive compound found in the rhizomes of *Curcuma longa* L.,<sup>32</sup> is one of the most thoroughly investigated natural product, as documented by studies claiming its efficacy and safety for both the prevention and treatment of various disorders.<sup>33,34</sup> This pharmacological pleiotropic behavior has been proposed to be strictly related to its mechanism of action that consists in a synergistic binding to different target proteins involved in related signaling pathways. For instance, the molecular basis of curcumin-mediated neuroprotection revealed the participation of a wide range of AD interrelated pathways, namely, aggregation of A $\beta$  and tau proteins, oxidative stress, and neuroinflammation.<sup>35</sup> Moreover, from a medicinal chemistry standpoint, the curcumin pharmacophore proved to be an excellent lead for the design of analogues with improved biological profile.<sup>36</sup>

Several investigations have been focused on curcumin tautomeric behavior, from a theoretical point of view, and the structure of curcumin in solution has been represented as an interconverting mixture of the symmetric diketo tautomer **1a** (1*E*,6*E*-1,7-bis-4-hydroxy-3-methoxyphenylhepta-1,6-diene-3,5-dione) and the asymmetric  $\beta$ -keto-enol tautomer **1b** (1*E*,4*Z*,6*E*-5-hydroxy-1,7-bis-4-hydroxy-3-methoxyphenylhepta-1,4,6-trien-3-one) (Figure 1). More recent theoretical and spectroscopic studies clearly provided evidence that **1b** is the predominant form in a wide range of organic solvents and buffered solutions

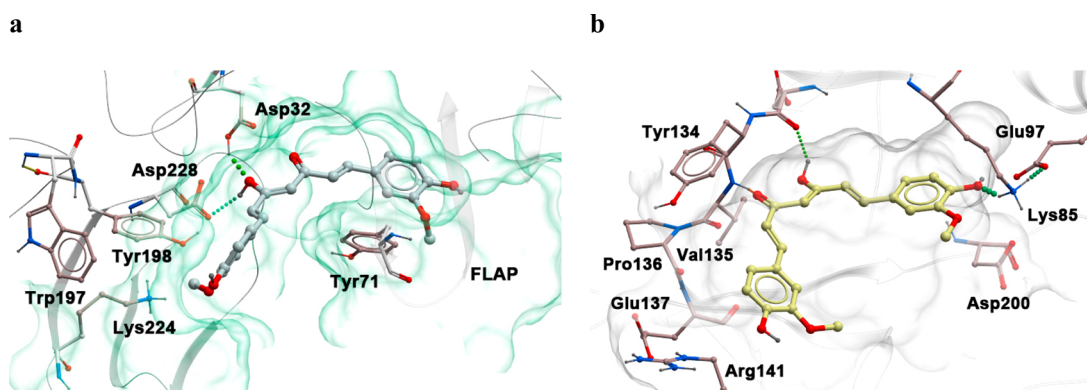
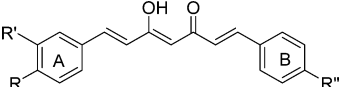


Figure 2. Curcumin 1b docked into the catalytic region of (a) BACE-1 and (b) GSK-3 $\beta$ .

Table 1. Inhibition of BACE-1 and GSK-3 $\beta$  Enzymatic Activities by the Curcumin-Based Analogues as the  $\beta$ -Keto-enol Tautomer (2–12) and Reference Compound Curcumin (1b)

					IC <sub>50</sub> ( $\mu$ M) <sup>a</sup> ± SEM	
comp	R	R'	R''		BACE-1	GSK-3 $\beta$
2	OH	OCH <sub>3</sub>			0.97 ± 0.43	0.90 ± 0.38
3	OH	OCH <sub>3</sub>	CH <sub>3</sub>		0.14 ± 0.03	2.09 ± 0.51
4	OH	H	OH		2.54 ± 0.02 17 ± 3 <sup>c</sup>	8.39 ± 1.59
5	OCH <sub>3</sub>	H	OCH <sub>3</sub>		1.65 ± 0.01	0.53 ± 0.27
6		H	OCH <sub>3</sub>		2.28 ± 0.64	2.78 ± 0.44
7		H	OH		2.69 ± 1.01	2.01 ± 0.71
8		H			0.04 ± 0.01	2.49 ± 0.82
9		H			0.40 ± 0.06	9.63 ± 0.21
10		H			0.39 ± 0.34	8.30 ± 0.54
11		H			1.04 ± 0.34	12.81 ± 0.14
12		H			1.08 ± 0.66	16.99 ± 2.68
Curc (1b)					n.i. <sup>b</sup> 343 ± 45 <sup>c</sup>	17.95 ± 1.03

<sup>a</sup>Values are the mean ± SD of two independent measurements, each performed in triplicate. SEM = standard error of the mean. <sup>b</sup>n.i.: not inhibiting up to 3  $\mu$ M. <sup>c</sup>Data were taken from ref 41.

due to the stabilizing effect of the intramolecular H-bond on the  $\alpha,\gamma$ -unsaturated-keto-enol moiety (Figure 1), a property

that may play a critical role in determining its affinity to biological targets.<sup>37,38</sup>

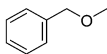
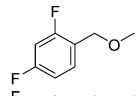
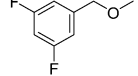
**Rational Design of Dual BACE-1 and GSK-3 $\beta$  Inhibitors.** Notwithstanding the fact that BACE-1 and GSK-3 $\beta$  are structurally unrelated enzymes and greatly differ in both three-dimensional structures and binding site topologies, we rationally envisaged the 5-hydroxy-1,7-diarylhepta-1,4,6-trien-3-one framework (main backbone of **1b**) as an appropriate structural element for their simultaneous modulation. In particular, the  $\beta$ -keto-enol central core of curcumin looked suitable for the interaction with BACE-1 catalytic dyad (Asp32 and Asp228), whereas the highly electrophilic  $\alpha,\beta$ -unsaturated carbonyl system, a well-known Michael acceptor system,<sup>39</sup> could covalently interact with the crucial Cys199 residue of GSK-3 $\beta$ .

To substantiate this hypothesis, the interactions of curcumin **1b** with the binding pocket of both targets were investigated by means of docking simulations (Figure 2a and b). Figure 2a shows how in, BACE-1 catalytic pocket, the central core was hydrogen bonded to the crucial Asp32 and Asp228 residues, while the side aryl rings established contacts with Tyr198, Lys224, and Tyr71. Figure 2b reports the predicted binding affinities of **1b** at GSK-3 $\beta$  binding pocket that were in good agreement with a previously proposed binding mode.<sup>40</sup> In particular, a number of significant interactions were established, and, namely, the central  $\beta$ -keto-enol function participated in a H-bond with Tyr134 and Val135, and the two aryl functions contacted Lys85, Glu97, and Arg141, and Glu173, respectively.

Furthermore, we tested the naturally occurring curcumin (**1b**) and its simplified analogue bis-demethoxycurcumin (**4**) for their ability to inhibit both BACE-1 and GSK-3 $\beta$  enzymes (Table 1). With regard to BACE-1 inhibition, curcumin proved to have moderate potency, while low-micromolar activity was observed for **4**, confirming previously reported data.<sup>41</sup> In the GSK-3 $\beta$  inhibition assay, both compounds proved to analogously modulate the enzyme (micromolar IC<sub>50</sub> values). In summary, **4** showed a promising dual BACE-1/GSK-3 $\beta$  inhibitory profile (2.54  $\mu$ M and 8.39  $\mu$ M on BACE-1 and GSK-3 $\beta$ , respectively). Taken together, these initial investigations confirmed the suitability of the curcumin scaffold for the development of effective dual BACE-1 and GSK-3 $\beta$  inhibitors.

To explore the chemical space of the two targets and perform a preliminary structure–activity relationship (SAR) study, a small library of curcumin-based analogues (Figure 1) was designed and synthesized. Different moieties were introduced on the side aryl functions of the main scaffold, while the central heptadienone fragment was retained. The choice of the substituents was mainly addressed to favor the crossing of the blood–brain barrier (BBB), as this pharmacokinetic property represents an essential requirement for drugs targeting CNS. The new curcumin-based analogues were primarily screened on BACE-1 and GSK-3 $\beta$  enzymes to determine their inhibitory profiles (Tables 1 and 2). Subsequently, for the most promising compounds, in terms of inhibitory activities (high potency against one target or balanced inhibitory profile on both targets), the AD-modifying profile, namely, neuroprotection, potential neurotoxicity, and ability to cross the BBB, were also investigated. Moreover, docking simulations were performed, in order to study the general positioning of this new series within the active site of both targets and to assess specific interactions with the residues of the catalytic pockets. To this aim, we selected **8** and **5** as the most potent BACE-1 and GSK-3 $\beta$  inhibitors of the series, respectively, and **2**, **4**, **6**, and **7** as low-micromolar dualistic inhibitors.

**Table 2.** Inhibition of BACE-1 and GSK-3 $\beta$  Enzymatic Activities by the Curcumin-Based Analogues as the Diketo Tautomer (**13–16**)

		IC <sub>50</sub> ( $\mu$ M) <sup>a</sup> ± SEM	
comp	R	BACE-1	GSK-3 $\beta$
<b>13</b>	OCH <sub>3</sub>	> 5	15.30 ± 3.64
<b>14</b>		6.04 ± 0.57	5.56 ± 0.01
<b>15</b>		1.00 ± 0.35	9.06 ± 2.07
<b>16</b>		0.73 ± 0.24	9.66 ± 1.02

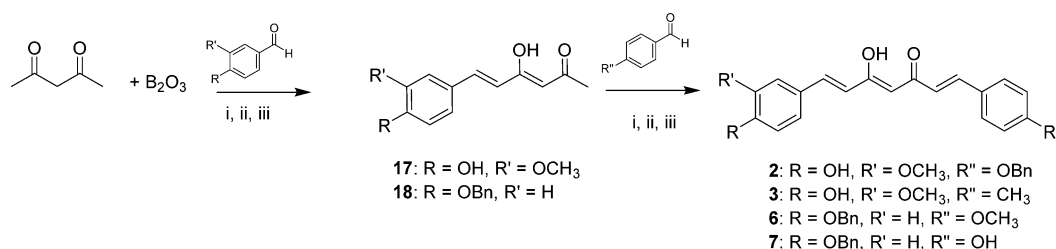
<sup>a</sup>Values are the mean ± SD of two independent measurements, each performed in triplicate. SEM = standard error of the mean.

**Chemistry.** The synthetic route for obtaining the target curcumin-based compounds (**1b–8**, **11**, and **12**) is outlined in Schemes 1 and 2, applying the Pabon reaction.<sup>42</sup> In summary, pentane-2,4-dione was complexed with B<sub>2</sub>O<sub>3</sub> in ethyl acetate (EtOAc) to avoid the methylene-centered reactivity toward the Knoevenagel reaction and to favor the nucleophilic attack at the side methyl groups. The boric complex was then condensed with the suitable aldehyde, and then a stepwise addition of *n*-tributylborate and *n*-butylamine was carried out. Acidic treatment allowed the complex to dissociate. This reaction has been reported to give curcumin as the  $\beta$ -keto-enol tautomer. The synthesis of the asymmetric curcumin-based analogues (**2**, **3**, **6**, and **7**) could be performed by condensing two different aldehydes, obtaining thus a complex mixture of compounds, among which are the asymmetrical and the two symmetrical curcuminoids, including the semireaction products (monoaryl curcumin). Consequently, obtaining the desired compounds in a good yield and purity grade would require several purification processes (column chromatography). To avoid this drawback, we performed the synthesis of the asymmetric curcumin analogues (Scheme 1) via a two-steps strategy, in which the monoaryl curcumin synthetic intermediates were first prepared under the classical reaction conditions, employing vanillin or 4-benzyloxybenzaldehyde (**17** and **18**, respectively). Subsequently, a second Pabon reaction, with a suitable aldehyde, allowed us to obtain the desired final compounds, maintaining the  $\beta$ -keto-enol tautomeric form. Scheme 2 reports the synthetic one-pot Pabon reaction procedure for obtaining the symmetrical analogues, by using a stoichiometric ratio of 1:1.8 for acetylacetone and the selected substituted benzaldehyde (**4**, **5**, **8**, **11**, and **12**).

The Williamson ether synthesis (Scheme 3) between a phenol-key intermediate (**4**) and a selected benzyl halide, in the presence of K<sub>2</sub>CO<sub>3</sub> as base, gave the desired products in a mixtures of  $\beta$ -keto-enol (**8–10**) and symmetric diketo tautomers (**14–16**). In particular, the alkaline reaction conditions induced a transformation of the  $\beta$ -keto-enol tautomer into the corresponding diketo one. Moreover, the employment of a

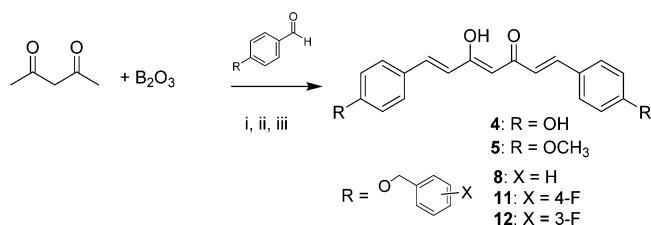


**Scheme 1. General Synthetic Method for Mono-aryl Curcumin Intermediates (17 and 18) and Asymmetric Curcumin-Based Analogues (2, 3, 6, and 7)<sup>a</sup>**



<sup>a</sup>Reagents and conditions: (i) B(*n*-BuO)<sub>3</sub>; (ii) *n*-BuNH<sub>2</sub>, 80 °C; (iii) HCl, 80 °C.

**Scheme 2. General Synthetic Method for Symmetric Curcumin-Based Analogues 4, 5, 8, 11, and 12<sup>a</sup>**



<sup>a</sup>Reagents and conditions: (i) B(*n*-BuO)<sub>3</sub>; (ii) *n*-BuNH<sub>2</sub>, 80 °C; (iii) HCl, 80 °C.

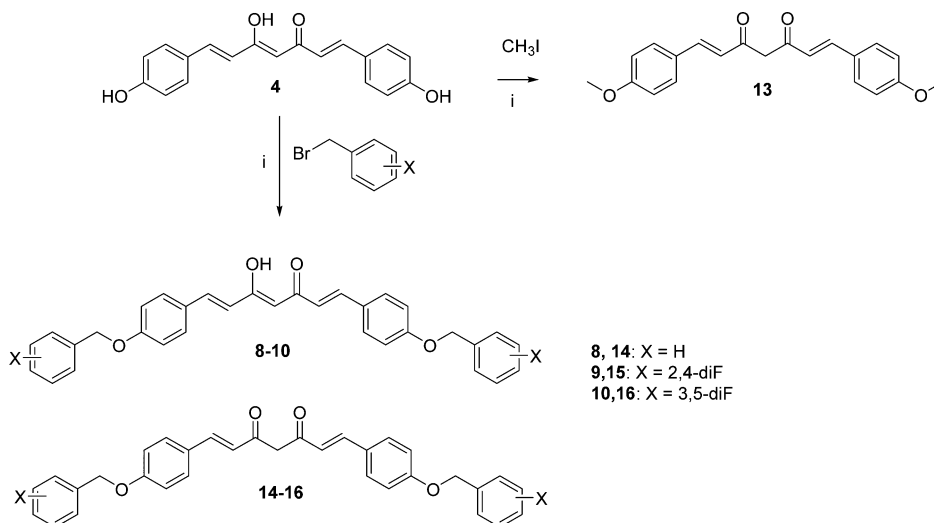
sterically demanding alkylating reagent was essential for obtaining both the tautomeric ethers into the reaction mixture. Additionally, these encumbering chemical features provided each reaction product with a fairly different chromatographic behavior, and as a consequence, each single tautomer could then be successfully and carefully isolated from the crude reaction by flash column chromatography and further purified by crystallization from a suitable solvent, thus obtaining the target compound in high purity grade. Interestingly, when methyl iodide was used as the alkylating reagent (Scheme 3), it was not possible to obtain the corresponding tautomers 5 and 13 as chromatographically different compounds, and to avoid separation difficulties, reaction time was lengthened in order to

convert 5 into 13; a byproduct was also separated and identified. This type of reaction also allowed us to study the stability of the synthesized derivatives (see [Chemical Stability Studies](#)).

## RESULTS AND DISCUSSION

**BACE-1 and GSK-3 $\beta$  Inhibition. BACE-1 Inhibition.** The ability to inhibit BACE-1 enzyme activity was investigated by means of a biochemical assay performed using the fluorescence resonance energy transfer (FRET) methodology<sup>43</sup> and using curcumin as the reference compound. The results are reported in [Tables 1](#) and [2](#). All of the tested compounds 2–16 turned out to effectively inhibit BACE-1, more than 1b (in our *in vitro* test, it did not inhibit this enzyme up to 3  $\mu$ M) with IC<sub>50</sub> ranging from nanomolar to low micromolar values. These good potencies confirmed the suitability of the curcumin main framework for BACE-1 inhibition, substantiating the design rationale for this target, even if the nature of the substituents on the side aryl functions seemed to have an intense effect on activity. The structurally closely related 2 and 3, bearing curcumin's 4-hydroxy-3-methoxyphenyl as the A ring, and a 4-benzyloxyphenyl or *para*-tolyl as the B ring, respectively, proved to effectively inhibit BACE-1 (IC<sub>50</sub> values of 0.97 and 0.14  $\mu$ M, respectively). The corresponding bis-*para*-benzyloxyphenyl symmetrical analogue 8 showed high potency, and, with an IC<sub>50</sub> value of 40 nM, was the most active compound of the series. A remarkable drop in potency (2 orders of

**Scheme 3. General Synthetic Method for Diketo Tautomer 13 and Tautomeric Couples 8 and 14, 9 and 15, and 10 and 16<sup>a</sup>**



<sup>a</sup>Reagents and conditions: (i) K<sub>2</sub>CO<sub>3</sub>, acetone, 80 °C.

magnitude) was observed for the corresponding diketo tautomer (**14**). The docked pose of **8** at the BACE-1 binding site (Figure S1a in Supporting Information) was in good agreement with the reported activity, as the molecule spanned the enzyme active site and the benzyloxy rings pointed toward both the S and the S' subpockets, binding the hydrophobic region described by the side chains of aromatic residues (Tyr198) and the flap region. From this structure-based docking simulation, it was evident that, to maintain this optimal binding mode, the benzyl rings of **8**-based analogues could only be decorated with small substituents, such as a fluorine atom. The latter, when strategically positioned, has been reported to positively affect the biological profile in terms of enhanced binding interaction, metabolic stability, and selective reactivity<sup>44</sup> allowing the development of effective BACE-1 inhibitors.<sup>45,28</sup> Symmetrically fluorinated **8**-analogues were synthesized, a lower potency (1 order of magnitude) relative to **8** was observed for compounds **9** and **10** (2,4-di-F and 3,5-disubstituted analogues,  $IC_{50}$  = 0.40 and 0.39  $\mu$ M, respectively), and a further drop in activity was documented for **11** and **12** (4-F and 3-F substituted analogues,  $IC_{50}$  = 1.04 and 1.08  $\mu$ M, respectively). For this subset, the corresponding diketo tautomers of the difluorinated **9** and **10** (**15** and **16**), as the most active compounds of the series, showed only a moderate decrement of activity. When one or both benzyloxy moieties of **8** were replaced by methoxy and hydroxy (**4**–**7**), low micromolar inhibitory potencies were observed. Analogously to **14**, the 5-diketo tautomer (**13**) was less active than the corresponding  $\beta$ -keto-enol. Taken together, these data pointed out that the structural modifications on **8** had, in general, detrimental effects on BACE-1 inhibiting activity.

**GSK-3 $\beta$  Inhibition.** A luminescent assay was employed for the evaluation of the GSK-3 $\beta$  inhibitory potency.<sup>46</sup> The curcumin-based analogues (**2**–**16**) showed a narrower GSK-3 $\beta$  inhibition range compared to that observed for BACE-1 ( $IC_{50}$  values from 0.53 to 16.99  $\mu$ M). All of the tested compounds showed micromolar activities, except for the *para*-methoxy substituted **5**, with an  $IC_{50}$  value of 0.53  $\mu$ M, that proved to be the most active in the series, more potent than **1b** ( $IC_{50}$  = 17.95  $\mu$ M) and **4** ( $IC_{50}$  = 8.39  $\mu$ M). Good GSK-3 $\beta$  inhibition was also obtained with the replacement of a side aryl ring of curcumin with a *para*-benzyloxyphenyl or a *para*-tolyl functions (**2** and **3**,  $IC_{50}$  = 0.90 and 2.09  $\mu$ M, respectively). Moreover, **8**, **6**, and **7**, all bearing a *para*-benzyloxyphenyl moiety, showed similar inhibitory potencies (around 2  $\mu$ M). A lowered inhibitory potency was observed for the **8**-based fluorinated subset ( $IC_{50}$  values ranging from 8.30 to 16.99  $\mu$ M) that proved to be slightly more active or as active as **1b**. Concerning the diketo tautomers, only for **13** a notable divergence in activity was observed with respect to the  $\beta$ -keto-enol counterpart, for the other compounds of this series bearing *para*-benzyloxyphenyl groups (**14**, **15**, and **16**) only a moderate decrease in activity was observed.

In light of these results, among the tested compounds **8** and **5** proved to be the most potent BACE-1 and GSK-3 $\beta$  inhibitors, respectively. A well-balanced dual low-micromolar inhibition profile was observed for **2**, **6**, and **7**, thus offering promises for gaining ground in the development of curcumin-based multitarget drug candidates for AD treatment.

**Computer-Assisted Studies.** Aimed at gaining insight into the molecular determinants of the curcumin-based analogues involved in effective interactions with BACE-1 and GSK-3 $\beta$  binding sites, docking studies were performed. To this aim, **8**

and **5** were selected as highly active principally on one of the two targets and **6** and **7** as balanced inhibitors on both targets (see Supporting Information for the binding mode description and for Figures S1a–d and S2a–d displaying docking predictions). We subsequently carried out molecular docking simulations to study the interactions of the balanced low-micromolar inhibitor **2** with the catalytic pocket of both targets. (Figures S3a and S3b).

**Covalent Docking Simulation on GSK-3 $\beta$ .** Taking into account the frequently claimed strong correlation between the compound's reactivity and bioactivity, and the highly and well established electrophilic properties of the curcumin pharmacophore, a covalent docking was accomplished in which a thia-Michael reaction occurred by nucleophilic attack of GSK-3 $\beta$  Cys199 residue on the reactive  $\alpha,\beta$ -unsaturated carbonyl function of **5** (Figure 3). It can be speculated that specific

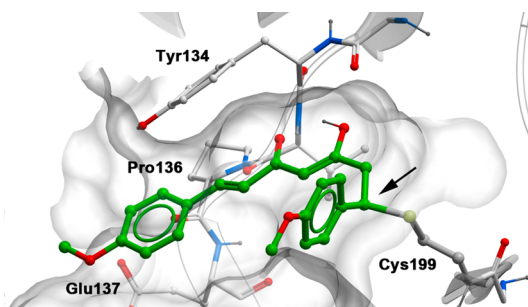


**Figure 3.** Predicted covalently bound conformation of **5** at the binding site of GSK-3 $\beta$ . Covalent docking was accomplished in which a thia-Michael reaction occurred by nucleophilic attack of GSK-3 $\beta$  Cys199 residue on the reactive  $\alpha,\beta$ -unsaturated carbonyl function of **5** (black arrow). The conformation then adopted by **5** stabilizes even further the interactions within the hinge region of GSK-3 $\beta$ . The covalently bound ligand is reported in green x-sticks. The key residues of the hinge region and Cys199 are reported in light gray x-sticks and labeled explicitly.

noncovalent interactions of the molecule with the binding pocket of the target are critical for the optimal orientation of the electrophile pharmacophore toward a specific protein nucleophile residue, thus increasing the speed and selectivity of the interaction (covalent bond).<sup>47</sup>

**Thiol Trapping Assay.** To support the covalent docking study, a spectroscopic <sup>1</sup>H NMR-based thiol trapping assay was performed. This procedure has been described for several electrophilic compounds, among them curcumin,<sup>48</sup> that was reported to irreversibly and quickly react with cysteamine in DMSO-*d*<sub>6</sub> to afford the corresponding bis-1,7-thia-Michael adduct, as documented by the disappearance of the olefin signals on the <sup>1</sup>H NMR spectra.<sup>49</sup> Compound **5** underwent a thiol-trapping reaction by employing a mixture of **5**/cysteamine in a 1:2 stoichiometric ratio,<sup>48</sup> affording the corresponding thia-Michael adduct in a very short time as documented in Figure 4. Analogously, competitive experiments were also carried out on **2**, **8**, and **6**; longer times of reaction were observed, with respect to **5**, with the following reactivity order: **5** > **2** > **6**–**8**, suggesting a potential detrimental effect on reactivity elicited by the benzyloxy function, partially compensated by the presence of the 4-OH, 3-OCH<sub>3</sub>-phenyl ring (**2**).

**Chemical Stability Studies.** A number of studies provided evidence about curcumin's poor stability in aqueous solutions at physiological pH, and several degradation products were identified.<sup>50,51</sup> The chemical stability of **5** as  $\beta$ -keto-enol form

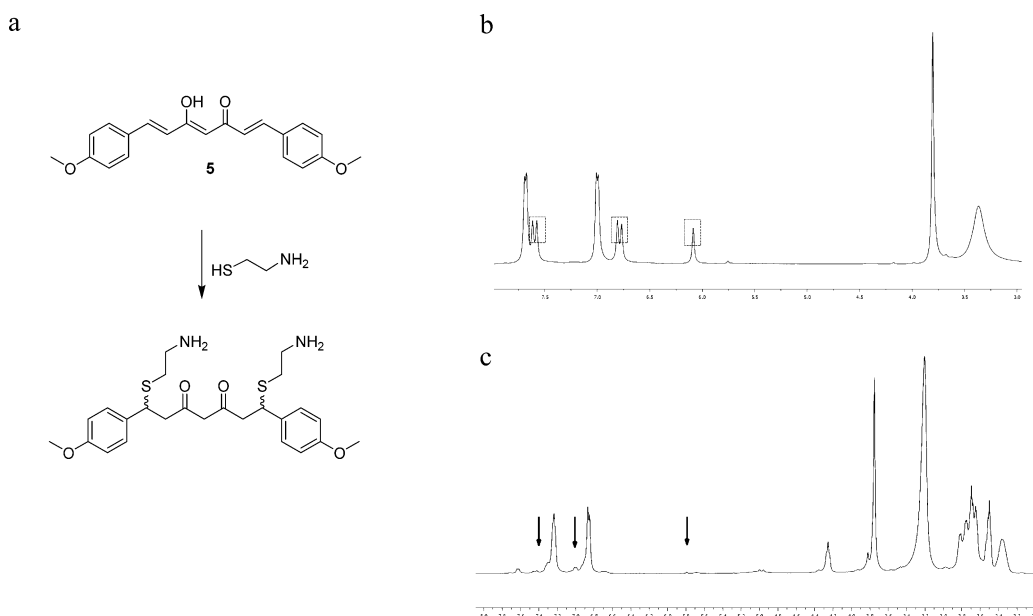


**Figure 4.** Thiol trapping assay. (a) Reaction of **5** with cysteamine. (b)  $^1\text{H}$  NMR spectrum of **5** in  $\text{DMSO}-d_6$ . In the squares, the signals of the  $\alpha,\gamma$ -unsaturated-keto-enol system are indicated. (c)  $^1\text{H}$  NMR spectrum of the **5**-positive assay, in  $\text{DMSO}-d_6$ , with a 1:2 stoichiometric ratio of **5**/cysteamine. The arrows indicate the disappearance of the above-mentioned signals.

and its diketo tautomeric counterpart **13**, together with their potential interconversion, were studied by RP-HPLC. For **5**, in the working conditions, no degradation or tautomeric conversion was observed. On the contrary, by analyzing the DMSO solution of **13** the formation of a degradation product was noted. This derivative was separated from the mixture, and its structure was determined by  $^1\text{H}$  NMR spectroscopy and (ESI-MS) as the diketene derivative (1*E*,4*E*-1,5-bis-4-methoxyphenylpenta-1,4-dien-3-one), endorsing curcumin's reported behavior.<sup>51</sup> On the contrary, **14** and the fluorinated-benzyloxy derivatives, obtained with a synthetic route similar to that of **13**, showed good chemical stability, and no degradation product was observed during the purification procedure. The presence of the benzyloxy functions seemed to strongly increase compound stability.

**Blood–Brain Barrier (BBB) Permeation.** One of the main obstacles for the treatment of the diseases of the CNS is the drug's penetration into BBB at therapeutic concentrations. The BBB is a complex interface between the blood and the CNS that strictly controls exchanges between the two compartments.<sup>52</sup> This barrier is composed of endothelial cells with tight junctions that protect the brain from endogenous materials which could damage brain tissues.<sup>53</sup> The majority of CNS drugs enter the brain by transcellular passive diffusion, due to the tight junction structure and limited transport pathways. In early drug discovery stage, evaluation of ADME (Absorption, Distribution, Metabolism, Excretion) properties is of crucial importance to reduce attrition in the development process. The Parallel Artificial Membrane Permeability Assay (PAMPA) is a high throughput technique developed to predict passive permeability through biological membranes. As curcumin and its metabolites were reported to have poor BBB permeability,<sup>54</sup> it seemed to be significant to evaluate the new derivatives for their impact on BBB crossing. Thus, the capacity of the selected candidates (**2–6** and **8**) to penetrate into the CNS was examined through the PAMPA-BBB method described by Di et al.,<sup>55</sup> using curcumin (**1b**) as standard. The *in vitro* permeability

(*Pe*) values were determined, expressed as  $10^{-6} \text{ cm} \cdot \text{s}^{-1}$ , and reported in Table 3. In light of the guidelines previously

**Table 3.** Permeability (*Pe*  $10^{-6} \text{ cm} \cdot \text{s}^{-1}$ ) in the PAMPA-BBB Assay for the Selected Compounds (**1b**, **2–6**, and **8**) with Their Predictive Penetration in the CNS

compd <sup>a</sup>	<i>Pe</i> ( $10^{-6} \text{ cm} \cdot \text{s}^{-1}$ ) <sup>b</sup>	prediction
<b>2</b>	$7.7 \pm 1.8$	CNS +
<b>3</b>	$8.2 \pm 1.3$	CNS +
<b>4</b>	$7.8 \pm 0.2$	CNS +
<b>5</b>	$2.8 \pm 0.3$	CNS + /CNS –
<b>6</b>	$7.0 \pm 0.7$	CNS +
<b>8</b>	$3.6 \pm 0.1$	CNS + /CNS –
curc ( <b>1b</b> )	$2.5 \pm 0.1$	CNS + /CNS –

<sup>a</sup>PBS/EtOH (70:30) was used as solvent. <sup>b</sup>Data are the mean  $\pm$  SD of 2 independent experiments.

established for the prediction of BBB permeation,<sup>56</sup> compounds with a *Pe* value superior than  $4.22 \times 10^{-6} \text{ cm} \cdot \text{s}^{-1}$  could be considered as capable of crossing the BBB and classified as CNS + ; a borderline profile was reported as CNS + /CNS –. The results indicate that compounds **2**, **3**, **4**, and **6** may pass the BBB, while **5** and **8** showed a borderline behavior.

**Neuroprotection.** The neuroprotective potential was also investigated for some selected compounds by evaluating (i) antioxidant properties, (ii) induction of the detoxifying enzyme NAD(P)H:quinone oxidoreductase 1 (NQO1), and (iii) cell viability. Curcumin (**1b**) was employed as the lead compound.

(i). **Antioxidant Properties.** Oxidative stress has been recognized as a common pathological feature in AD. It is substantially produced by reactive radical species, among others reactive oxygen species (ROS), together with the loss of function of many antioxidant defense enzymes that cause imbalance between the formation of cellular oxidants and the antioxidative processes.<sup>57</sup> Compounds able to inactivate these entities could promise valuable therapeutic efficacy. The ability

of the selected curcumin-based derivatives **2**, **3**, and **8**, together with **1b**, to protect from oxidative stress was studied on T67 cells by evaluating their ROS scavenging ability after exposure to 100  $\mu\text{M}$  *tert*-butyl hydroperoxide (TBH) at the fixed concentration of 10  $\mu\text{M}$  (Figure 5). The results showed that **2**

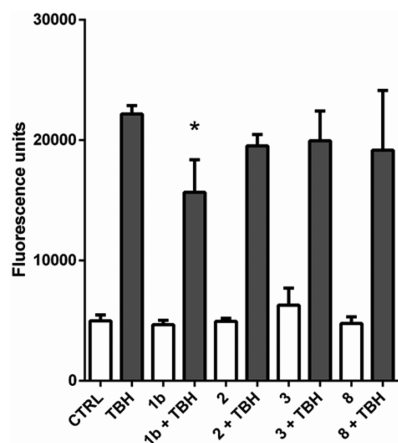


**Figure 5.** Effect of compounds **1b**, **2**, **3**, and **8** on ROS formation in T67 cells. The antioxidant potential was estimated as ROS scavenging ability. The cells treated with compounds at the fixed concentration of 10  $\mu\text{M}$  were exposed to 100  $\mu\text{M}$  TBH. The increase in DCFDA fluorescence is related to the intracellular ROS formation. Data are reported as the mean  $\pm$  standard deviation of at least three independent experiments. \*  $p \leq 0.05$ , ( $n = 3$ ).

maintained a moderate scavenging activity, slightly lower than curcumin's ( $P = 0.005$  for curcumin vs TBH and  $P = 0.08$  for **2** vs TBH), while **3** and **8**, although displaying the same mean value, showed a higher standard deviation that makes them not statistically significant. The lack of scavenging activity observed for **3** suggested that this property could not only be ascribed to the presence of the 3-OCH<sub>3</sub>,4-OH-phenyl function. This hypothesis was further confirmed as compounds **4**–**7** were quite ineffective when subjected to the same evaluation (see Figure S5).

(ii). **NQO1 Induction.** Human NQO1, a flavoprotein constitutively expressed in several tissues and organs, among which is the brain, exerts antioxidant effect by catalyzing the reduction of quinones to hydroquinones and by scavenging superoxide molecules.<sup>58</sup> In AD, as a result of a defense mechanism against increased oxidative stress, the levels of this phase 2 cytoprotective enzyme were found to be remarkably increased. Interestingly, an elevated expression of this enzyme has also been proposed as a first indicator of the pathology.<sup>59</sup> Its induction may correlate with a protective role by allowing one to delay the progression of the malady. As curcumin itself was demonstrated to effectively induce NQO1,<sup>60</sup> a set of representative derivatives (**2**–**8**) were selected to be tested on NQO1 induction potential by using **1b** as lead compound. As shown in Figure 6, the tested compounds proved to be NQO1 inducers. In particular, **8** and **4** were as active as curcumin, while higher activities were observed for **2**, **3**, and **6**. Notably, this effect has recently been demonstrated to slow the A $\beta$ -induced neurodegeneration in mice.<sup>61</sup>

(iii). **Neuronal Cell Toxicity.** Cytotoxic effects in several *in vitro* or *in vivo* models have been reported for curcumin.<sup>62</sup> The neurotoxic potential was thus examined for some selected compounds, namely, **1b** and **2**–**8**. Cells were exposed to compound concentrations ranging from 0 to 20  $\mu\text{M}$  for a 24 h

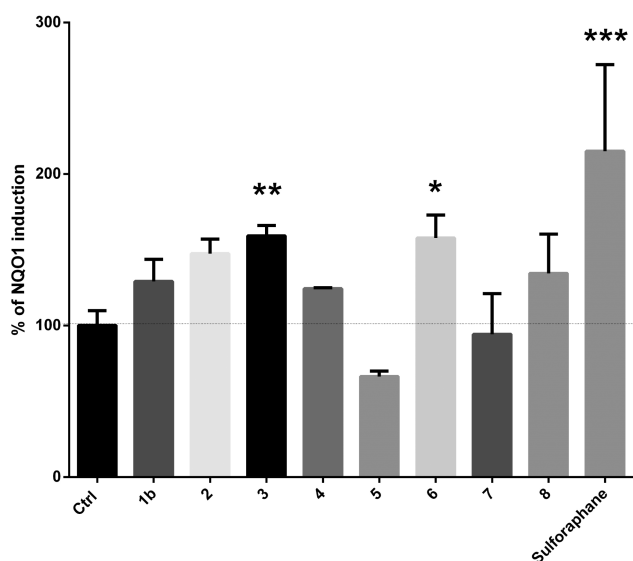


**Figure 6.** NQO1 induction in T67 cells by treatment with 10  $\mu\text{M}$  curcumin **1b**, analogues **2**–**8**, and sulforaphane (2.5  $\mu\text{M}$ ), a potent NQO1 inducer used as the positive control. Data are reported as a percentage of dicumarol-inhibitable NQO1, setting at 100% the activity measured in untreated cells (Ctrl). Data are reported as the mean  $\pm$  standard deviation of at least three independent experiments. \*  $p \leq 0.05$ ; \*\*  $p \leq 0.01$ ; \*\*\*  $p \leq 0.001$ , ( $n = 4$ ) in comparison with control cells (Ctrl).

period of time, and cell viability was measured by the MTT test, with **1b** as the lead compound. As shown in Figure 7, in the

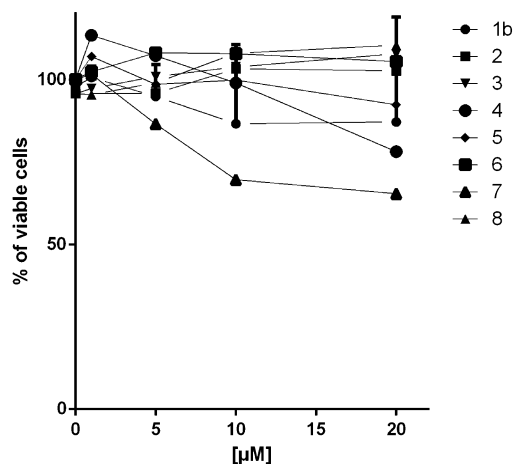


**Figure 7.** Cytotoxicity of compounds **1b**, **2**–**8**. The toxic effect in T67 cell lines, was estimated by the MTT assay after 24 h of treatment. Results are expressed as the percentage of viable cells and are the mean  $\pm$  SE of four different experiments run at least in quadruplicate.

experimental conditions, when increasing the concentration of the tested compound, no remarkable decrease of cell viability was observed. In particular, **4** and **7** showed moderate toxicity at 20  $\mu\text{M}$  concentration, comparable to that of **1b**, and that for **7** was dose-dependent. The remaining compounds did not show any apparent cytotoxic effects at these concentrations. The potential toxicity of **5**, **4**, and **6** was assayed only at the concentration of 10  $\mu\text{M}$  after 24 h of incubation, and the results confirmed the absence of any apparent cytotoxic effect.



## CONCLUSIONS

The complex pathological mechanisms of AD directed attention to polypharmacological strategies and multitarget drugs that acting on several targets involved in the disease could promise improved effectiveness compared to that of single-target drugs. In this scenario, BACE-1 and GSK-3 $\beta$  emerged as AD validated targets. The curcumin pharmacophore, in its  $\beta$ -keto-enol form, encompassing some structural features suitable for modulation of BACE-1 and GSK-3 $\beta$ , was rationally envisaged as a potential dualistic inhibitor of both targets. Efforts addressed to the design and synthesis of a small library of curcumin-based analogues allowed us to obtain valuable probes to explore the chemical space of these structurally unrelated enzymes. Overall, the enol tautomeric form demonstrated to be an important feature for achieving good inhibitory potency and chemical stability. In summary, derivative **8** showed a remarkable gap of potency (2 orders of magnitude) between its inhibition of BACE-1 and GSK-3 $\beta$ . It indeed turned out to be a single-target inhibitor of BACE-1, but it could very well represent a promising starting point for the development of optimized dual modulators. Compounds **3**, **9**, and **10**, likewise characterized by higher potencies on BACE-1 with respect to GSK-3 $\beta$  (submicromolar and low-micromolar IC<sub>50</sub> values, respectively), showed reduced deviation from the dualistic profile. Interestingly, a number of derivatives proved to modulate BACE-1 and GSK-3 $\beta$  enzymes with quite comparable potencies in the micromolar range. A mild dualistic profile was shown for **4** and **5**, whereas **2**, **6**, and **7** proved to be well-balanced low-micromolar inhibitors of both enzymes, a crucial achievement in the multitarget drug discovery context. Furthermore, among this last subset, **2**, **3**, and **6** proved to induce NQO1 enzyme, thus promising to exert neuroprotective activity by counteracting the oxidative stress, a common feature of AD. In particular, **2**, thanks to its weak antioxidant effect accompanied by the absence of evident neurotoxic effects and by favorable pharmacokinetic behavior, clearly emerged as a promising AD-modifying drug candidate, and development of analogues derived from **2** will certainly be pursued.

In light of these findings, several curcumin-based analogues were identified in this study as valuable lead compounds that deserve attention to be optimized with different approaches, all aimed at obtaining effective and dualistic BACE-1/GSK-3 $\beta$  inhibitors, endowed with good neuroprotective and pharmacokinetic properties.

## EXPERIMENTAL SECTION

**Chemistry. General Procedures.** Starting materials, unless otherwise specified in this section, were high-grade commercial products. Solvents were of analytical grade. Melting points were determined in open glass capillaries using a Büchi apparatus and are uncorrected. <sup>1</sup>H NMR and <sup>13</sup>C NMR spectra were recorded on Varian Gemini, and chemical shifts are reported as parts per million (ppm  $\delta$  value) relative to the peak for tetramethylsilane (TMS) as internal standard. Standard abbreviations indicating spin multiplicities are given as follows: s (singlet), d (doublet), t (triplet), br (broad), q (quartet), or m (multiplet). Mass spectra were recorded on a Waters ZQ 4000 apparatus operating in electrospray mode (ES). Chromatographic separations were performed on silica gel columns using the flash method (Kieselgel 40, 0.040–0.063 mm, Merck). Reactions were followed by thin layer chromatography (TLC) on precoated silica gel plates (Merck Silica Gel 60 F254) and then visualized with a UV lamp. Satisfactory elemental analyses were obtained for all new compounds, confirming >95% purity. Compounds were named following IUPAC

rules as applied by Beilstein-Institute AutoNom (version 2.1), a PC-integrated software package for systematic names in organic chemistry.

**Pabon Reaction: General Synthetic Procedure for Compounds 1b–8, 17, and 18.** To a stirred solution of pentane-2,4-dione (1.00 mmol) in EtOAc (1.0 mL), B<sub>2</sub>O<sub>3</sub> (1.0 molar equiv) was added, and the suspension was stirred for 30 min at 80 °C before addition of a solution of the appropriate aldehyde/s (0.9 molar equiv for monoaryl or 1.8 molar equiv for biaryl curcumin derivatives) and tri-*n*-butyl borate (2.0 molar equiv for monoaryl or 4.0 molar equiv for biaryl curcumin derivatives) in EtOAc (0.5 mL). The reaction mixture was stirred at 80 °C for 30 min, then a solution of *n*-butylamine (0.4 molar equiv in 1.0 mL of EtOAc) was added over a period of 15 min. The mixture was heated to 80 °C for 8 h, and then, after cooling to r.t., it was acidified with 0.5 N HCl (30 mL) and then stirred at 80 °C for 30 min. The organic phase was separated, and the aqueous layer was extracted with EtOAc (3  $\times$  10 mL). The combined organic layers were sequentially washed with saturated aqueous NaHCO<sub>3</sub> and brine, dried over Na<sub>2</sub>SO<sub>4</sub>, filtered, and concentrated under reduced pressure. The crude residue was purified by flash column chromatography using a mixture of petroleum ether/ethyl acetate (PE/EtOAc) as eluent, followed by crystallization from suitable solvent.

With this procedure, the following compounds were obtained.

**3Z,5E-4-Hydroxy-6-(4-hydroxy-3-methoxyphenyl)hexa-3,5-dien-2-one (17).** Reaction of pentane-2,4-dione (1.00 g, 10.00 mmol), B<sub>2</sub>O<sub>3</sub> (0.70 g, 10.00 mmol), and vanillin (1.37 g, 9.00 mmol), in EtOAc (15.0 mL), gave a crude product that was purified by flash chromatography (PE/EtOAc, 9.75:0.25); yellow powder, 55% yield, mp 144–146 °C (EtOH). <sup>1</sup>H NMR (400 MHz, CDCl<sub>3</sub>):  $\delta$  2.16 (s, 3H, CH<sub>3</sub>), 3.94 (s, 3H, OCH<sub>3</sub>), 5.40 (br, 1H, OH), 5.63 (s, 1H, keto-enol-CH), 6.33 (d, 1H, *J* = 16.0 Hz, CH=CH), 6.92 (d, 1H, *J* = 8.0 Hz, H-5), 7.02 (d, 1H, *J* = 1.8 Hz, H-2), 7.09 (dd, 1H, *J* = 8.0 and 1.8 Hz, H-6), 7.53 (d, 1H, *J* = 16.0 Hz, CH=CH). Analytical data of this intermediate are in good agreement with the literature data.<sup>63</sup>

**3Z,5E-6-(4-Benzyloxyphenyl)-4-hydroxyhexa-3,5-dien-2-one (18).** Reaction of pentane-2,4-dione (1.00 g, 10.00 mmol), B<sub>2</sub>O<sub>3</sub> (0.70 g, 10.00 mmol), and 4-benzyloxybenzaldehyde (2.04 g, 9.00 mmol) gave a crude product that was purified by flash chromatography (PE/EtOAc, 9.95:0.05); yellow powder, 65% yield, mp 121–122 °C (DCM/PE). <sup>1</sup>H NMR (400 MHz, CDCl<sub>3</sub>):  $\delta$  2.18 (s, 3H, CH<sub>3</sub>), 5.20 (s, 2H, OCH<sub>2</sub>), 5.61 (s, H, keto-enol-CH), 6.33 (d, 1H, *J* = 16.0 Hz, CH=CH), 6.94 (d, 2H, *J* = 8.2 Hz, Ar), 7.40–7.45 (m, 5H, Bn), 7.53 (d, 2H, *J* = 8.2 Hz, Ar), 7.53 (d, 1H, *J* = 16.0 Hz, CH=CH).

**1E,4Z,6E-1-(4-Benzyloxyphenyl)-5-hydroxy-7-(4-hydroxy-3-methoxyphenyl)hepta-1,4,6-trien-3-one (2).** Reaction of **17** (1.17 g, 5.00 mmol), B<sub>2</sub>O<sub>3</sub> (0.35 g, 5.00 mmol), and 4-benzyloxybenzaldehyde (0.95 g, 4.50 mmol) gave a crude product that was purified by flash chromatography (PE/EtOAc, 9:1); orange-yellow powder, 44% yield, mp 169–170 °C (EtOH). <sup>1</sup>H NMR (400 MHz, CDCl<sub>3</sub>):  $\delta$  3.96 (s, 3H, OCH<sub>3</sub>), 5.19 (s, 2H, OCH<sub>2</sub>), 5.76 (s, 1H, keto-enol-CH), 6.45 (d, 2H, *J* = 16.0 Hz, CH=CH), 6.94 (d, 1H, *J* = 8.4 Hz, H-5), 6.98 (d, 2H, *J* = 8.4 Hz, Ar), 7.07 (d, 1H, *J* = 1.8 Hz, H-2), 7.12 (dd, 1H, *J* = 1.8 and 8.4 Hz, H-6), 7.40–7.45 (m, 5H, Bn), 7.53 (d, 2H, *J* = 8.4 Hz, Ar), 7.60 (d, 2H, *J* = 16.0 Hz, CH=CH). <sup>13</sup>C NMR (101 MHz, CDCl<sub>3</sub>):  $\delta$  55.70, 70.44, 103.56, 111.78, 115.81, 116.37 (2C), 123.18, 123.21, 127.58, 128.17 (3C), 128.32 (2C), 128.50 (2C), 129.01, 129.33, 137.27, 140.41 (2C), 148.50, 149.52, 160.78, 186.65 (2C). ESI-MS (*m/z*): 451 (M + Na).

**1E,4Z,6E-5-Hydroxy-7-(4-hydroxy-3-methoxyphenyl)-1-*p*-tolylhepta-1,4,6-trien-3-one (3).** Reaction of **17** (1.17 g, 5.00 mmol), B<sub>2</sub>O<sub>3</sub> (0.35 g, 5.00 mmol), and 4-methylbenzaldehyde (0.53 mL, 4.50 mmol) gave a product that was purified by flash chromatography (PE/EtOAc, 9:1); orange-yellow powder, 36% yield, mp 136–138 °C (EtOH). <sup>1</sup>H NMR (400 MHz, CDCl<sub>3</sub>):  $\delta$  2.38 (s, 3H, CH<sub>3</sub>), 3.95 (s, 3H, OCH<sub>3</sub>), 5.81 (s, 1H, keto-enol-CH), 6.49 (d, 1H, *J* = 15.8 Hz, CH=CH), 6.60 (d, 1H, *J* = 15.8 Hz, CH=CH), 6.94 (d, 1H, *J* = 8.2 Hz, H-5), 7.06 (d, 1H, *J* = 1.8 Hz, H-2), 7.13 (dd, 1H, *J* = 1.8 and 8.2 Hz, H-6), 7.20 (d, 2H, *J* = 8.0 Hz, Ar), 7.46 (d, 2H, *J* = 8.0 Hz, Ar), 7.59 (d, 1H, *J* = 15.8 Hz, CH=CH), 7.63 (d, 1H, *J* = 15.8 Hz, CH=CH). <sup>13</sup>C NMR (101 MHz, CDCl<sub>3</sub>):  $\delta$  21.04, 55.70, 107.59, 112.88, 116.00, 121.46, 121.87, 126.70, 127.42 (2C), 129.27 (2C), 130.94,

134.09, 141.23 (2C), 137.91, 148.50, 150.23, 183.70 (2C). ESI-MS ( $m/z$ ): 359 ( $M + Na$ ).

**1E,4Z,6E-7-(4-Benzyloxyphenyl)-5-hydroxy-1-4-methoxyphenylhepta-1,4,6-trien-3-one (6).** Reaction of **18** (1.47 g, 5.00 mmol),  $B_2O_3$  (0.35 g, 5.00 mmol), and 4-methoxybenzaldehyde (0.53 mL, 4.50 mmol) gave a crude product that was purified by flash chromatography (PE/EtOAc, 8:2); light orange-yellow powder, 48% yield, mp 135–137 °C (DCM/PE).  $^1H$  NMR (400 MHz,  $CDCl_3$ ):  $\delta$  3.86 (s, 3H,  $OCH_3$ ), 5.12 (s, 2H,  $OCH_2$ ), 5.80 (s, 1H, keto-enol-CH), 6.51 (d, 2H,  $J = 15.6$  Hz,  $CH=CH$ ), 6.93 (d, 2H,  $J = 8.0$  Hz, Ar), 7.00 (d, 2H,  $J = 8.0$  Hz, Ar), 7.40–7.45 (m, 5H, Bn), 7.52 (d, 4H,  $J = 8.0$  Hz, Ar), 7.63 (d, 2H,  $J = 15.6$  Hz,  $CH=CH$ ).  $^{13}C$  NMR (101 MHz,  $CDCl_3$ ):  $\delta$  55.41, 70.54, 114.68, 114.45 (2C), 115.30 (2C), 122.03, 127.80 (2C), 128.10 (2C), 128.50, 128.99 (2C), 129.79, 129.93 (4C), 137.02, 140.25 (2C), 160.73, 161.01, 183.49 (2C). ESI-MS ( $m/z$ ): 435 ( $M + Na$ ).

**1E,4Z,6E-7-(4-Benzyloxyphenyl)-5-hydroxy-1-4-hydroxyphenylhepta-1,4,6-trien-3-one (7).** Reaction of **18** (1.47 g, 5.00 mmol),  $B_2O_3$  (0.35 g, 5.00 mmol), and 4-hydroxybenzaldehyde (0.56 g, 4.50 mmol) gave a crude product that was purified by flash chromatography (PE/EtOAc, 9:1); yellow powder, 42% yield, mp 189–191 °C (EtOH).  $^1H$  NMR (400 MHz,  $CDCl_3$ ):  $\delta$  5.11 (s, 2H,  $OCH_2$ ), 5.78 (s, 1H, keto-enol-CH), 6.49 (d, 1H,  $J = 16.0$  Hz,  $CH=CH$ ), 6.50 (d, 1H,  $J = 15.6$  Hz,  $CH=CH$ ), 6.85 (d, 2H,  $J = 8.0$  Hz, Ar), 7.00 (d, 2H,  $J = 8.8$  Hz, Ar), 7.40–7.45 (m, 5H, Bn), 7.47 (d, 2H,  $J = 8.0$  Hz, Ar), 7.51 (d, 2H,  $J = 8.8$  Hz, Ar), 7.61 (d, 1H,  $J = 15.6$  Hz,  $CH=CH$ ), 7.62 (d, 1H,  $J = 15.6$  Hz,  $CH=CH$ ).  $^{13}C$  NMR (101 MHz,  $CDCl_3$ ):  $\delta$  70.70, 114.81, 115.70 (2C), 116.53 (2C), 122.57, 127.98 (2C), 128.21 (2C), 128.29, 129.04 (2C), 129.89, 130.06 (4C), 136.87, 140.74 (2C), 160.80, 161.00, 183.58 (2C). ESI-MS ( $m/z$ ): 421 ( $M + Na$ ).

**1E,4Z,6E-5-Hydroxy-1,7-bis-4-hydroxyphenylhepta-1,4,6-trien-3-one (4).** Reaction of pentane-2,4-dione (1.00 g, 10.00 mmol),  $B_2O_3$  (0.70 g, 10.00 mmol), and 4-hydroxybenzaldehyde (2.24 g, 18.00 mmol) gave a crude product that was purified by flash chromatography (PE/EtOAc, 7:3); red-orange powder, 88% yield, mp 228–230 °C (EtOH).  $^1H$  NMR (400 MHz, acetone- $d_6$ ):  $\delta$  5.99 (s, 1H, keto-enol-CH), 6.67 (d, 2H,  $J = 15.8$  Hz,  $CH=CH$ ), 6.91 (d, 4H,  $J = 8.6$  Hz, Ar), 7.57 (d, 4H,  $J = 8.6$  Hz, Ar), 7.61 (d, 2H,  $J = 15.8$  Hz,  $CH=CH$ ).  $^1H$  NMR (400 MHz,  $DMSO-d_6$ ):  $\delta$  6.22 (s, 1H, keto-enol-CH), 6.82 (d, 2H,  $J = 16.4$  Hz,  $CH=CH$ ), 6.98 (d, 4H,  $J = 8.4$  Hz, Ar), 7.25 (d, 4H,  $J = 8.4$  Hz, Ar), 7.35 (br, 1H, OH), 7.62 (d, 2H,  $J = 16.4$  Hz,  $CH=CH$ ), 9.70 (br, 2H, OH).  $^{13}C$  NMR (101 MHz, acetone- $d_6$ ):  $\delta$  114.00, 116.50 (4C), 122.86, 127.93 (2C), 129.71, 130.01 (4C), 141.08 (2C), 161.07 (2C), 183.50 (2C). ESI-MS ( $m/z$ ): 331 ( $M + Na$ ).

**1E,4Z,6E-5-Hydroxy-1,7-bis-4-methoxyphenylhepta-1,4,6-trien-3-one (5).** Reaction of pentane-2,4-dione (1.00 g, 10.00 mmol),  $B_2O_3$  (0.70 g, 10.00 mmol), and 4-methoxybenzaldehyde (2.19 mL, 18.00 mmol) gave a crude product that was purified by flash chromatography (PE/EtOAc, 9:1); yellow powder, 87% yield, mp 110–112 °C (DCM/PE).  $^1H$  NMR (400 MHz,  $CDCl_3$ ):  $\delta$  3.86 (s, 6H,  $OCH_3$ ), 5.79 (s, 1H, keto-enol-CH), 6.51 (d, 2H,  $J = 15.6$  Hz,  $CH=CH$ ), 6.93 (d, 4H,  $J = 7.2$  Hz, Ar), 7.52 (d, 4H,  $J = 7.2$  Hz, Ar), 7.63 (d, 2H,  $J = 15.6$  Hz,  $CH=CH$ ).  $^1H$  NMR (400 MHz,  $DMSO-d_6$ ):  $\delta$  3.80 (s, 6H,  $OCH_3$ ), 6.09 (s, 1H, keto-enol-CH), 6.79 (d, 2H,  $J = 15.6$  Hz,  $CH=CH$ ), 7.00 (d, 4H,  $J = 8.4$  Hz, Ar), 7.59 (d, 2H,  $J = 15.6$  Hz,  $CH=CH$ ), 7.68 (d, 4H,  $J = 8.4$  Hz, Ar).  $^{13}C$  NMR (101 MHz,  $CDCl_3$ ):  $\delta$  55.38 (2C), 113.75, 114.37 (4C), 121.80, 127.80 (2C), 129.51, 129.75 (4C), 140.09 (2C), 161.25 (2C), 183.33 (2C).  $^{13}C$  NMR (101 MHz,  $DMSO-d_6$ ):  $\delta$  55.38 (2C), 101.43, 114.52 (4C), 121.82 (2C), 127.33 (2C), 130.18 (4C), 140.05 (2C), 161.09 (2C), 183.12 (2C). ESI-MS ( $m/z$ ): 359 ( $M + Na$ ).

**1E,4Z,6E-1,7-Bis-4-benzyloxyphenyl-5-hydroxyhepta-1,4,6-trien-3-one (8).** Reaction of pentane-2,4-dione (1.00 g, 10.00 mmol),  $B_2O_3$  (0.70 g, 10.00 mmol), and 4-benzyloxybenzaldehyde (3.80 g, 18.00 mmol) gave a crude product that was purified by flash chromatography (PE/EtOAc, 9:1); yellow powder, 87% yield, mp 161–162 °C (DCM/PE).  $^1H$  NMR (400 MHz,  $CDCl_3$ ):  $\delta$  5.11 (s, 4H,  $OCH_2$ ), 5.78 (s, 1H, keto-enol-CH), 6.50 (d, 2H,  $J = 16.0$  Hz,  $CH=CH$ ), 6.99 (d, 4H,  $J = 8.4$  Hz, Ar), 7.40–7.44 (m, 10H, Bn), 7.51 (d, 4H,  $J = 8.4$  Hz, Ar),

7.62 (d, 2H,  $J = 16.0$  Hz,  $CH=CH$ ).  $^1H$  NMR (400 MHz,  $DMSO-d_6$ ):  $\delta$  5.17 (s, 4H,  $OCH_2$ ), 6.09 (s, 1H, keto-enol-CH), 6.79 (d, 2H,  $J = 16.4$  Hz,  $CH=CH$ ), 7.08 (d, 4H,  $J = 8.4$  Hz, Ar), 7.40–7.43 (m, 10H, Bn), 7.59 (d, 4H,  $J = 8.4$  Hz, Ar), 7.68 (d, 2H,  $J = 15.6$  Hz,  $CH=CH$ ).  $^{13}C$  NMR (101 MHz,  $CDCl_3$ ):  $\delta$  70.44 (2C), 115.61 (5C), 122.27, 127.79 (2C), 127.81 (2C), 128.39 (2C), 128.50 (2C), 128.98 (2C), 129.00 (2C), 130.07, 130.12 (4C), 136.80 (2C), 140.41 (2C), 160.78 (2C), 183.67 (2C). ESI-MS ( $m/z$ ): 511 ( $M + Na$ ).

**1E,4Z,6E-1,7-Bis-4-(4-fluorobenzyloxyphenyl)-5-hydroxyhepta-1,4,6-trien-3-one (11).** Reaction of pentane-2,4-dione (0.50 g, 5.00 mmol),  $B_2O_3$  (0.35 g, 5.00 mmol), and 4-(4-fluorobenzyloxybenzaldehyde **19** (2.07 g, 9.00 mmol) gave a crude product that was purified by flash chromatography (PE/EtOAc, 9:1); yellow solid, 31% yield, mp 210–212 °C.  $^1H$  NMR (400 MHz,  $CDCl_3$ ):  $\delta$  5.06 (s, 4H,  $OCH_2$ ), 5.78 (s, 1H, keto-enol-CH), 6.50 (d, 2H,  $J = 15.6$  Hz,  $CH=CH$ ), 6.98 (d, 4H,  $J = 8.8$  Hz, Ar), 7.09–7.13 (m, 4H, Ar), 7.41–7.44 (m, 4H, Ar), 7.51 (d, 4H,  $J = 8.8$  Hz, Ar), 7.62 (d, 2H,  $J = 15.6$  Hz,  $CH=CH$ ).  $^{13}C$  NMR (101 MHz,  $CDCl_3$ ):  $\delta$  70.89 (2C), 114.50, 115.01 (d, 4C,  $J = 27.3$  Hz), 115.72 (4C), 122.97, 128.89, 129.42 (4C), 129.47 (2C), 129.71 (d, 4C,  $J = 8.1$  Hz), 131.94 (d, 2C,  $J = 4.0$  Hz), 140.82 (2C), 159.67 (2C), 162.49 (d, 2C,  $J = 265.6$  Hz), 183.76 (2C). ESI-MS ( $m/z$ ): 547 ( $M + Na$ ).

**1E,4Z,6E-1,7-Bis-4-(3-fluorobenzyloxyphenyl)-5-hydroxyhepta-1,4,6-trien-3-one (12).** Reaction of pentane-2,4-dione (0.50 g, 5.00 mmol),  $B_2O_3$  (0.35 g, 5.00 mmol), and 4-(3-fluorobenzyloxybenzaldehyde **20** (2.07 g, 9.00 mmol) gave a crude product that was purified by flash chromatography (PE/EtOAc, 9:1); 35% yield, yellow solid, mp 160–162 °C.  $^1H$  NMR (400 MHz,  $CDCl_3$ ):  $\delta$  5.10 (s, 4H,  $OCH_2$ ), 5.78 (s, 1H, keto-enol-CH), 6.51 (d, 2H,  $J = 15.6$  Hz,  $CH=CH$ ), 6.98 (d, 4H,  $J = 8.8$  Hz, Ar), 7.01–7.05 (m, 2H, Ar), 7.16–7.18 (m, 2H, Ar), 7.20–7.22 (m, 2H, Ar), 7.35–7.37 (m, 2H, Ar), 7.51 (d, 4H,  $J = 8.8$  Hz, Ar), 7.62 (d, 2H,  $J = 15.6$  Hz,  $CH=CH$ ).  $^{13}C$  NMR (101 MHz,  $CDCl_3$ ):  $\delta$  72.62 (2C), 114.16 (d, 2C,  $J = 28.3$  Hz), 115.07 (d, 2C,  $J = 26.3$  Hz), 115.27 (5C), 123.31, 123.63 (d, 2C,  $J = 4.0$  Hz), 127.81 (4C), 128.99 (3C), 129.28 (d, 2C,  $J = 8.1$  Hz), 140.80 (d, 2C,  $J = 6.9$  Hz), 143.82 (2C), 160.59 (2C), 163.07 (d, 2C,  $J = 264.6$  Hz), 183.67 (2C). ESI-MS ( $m/z$ ): 547 ( $M + Na$ ).

**Williamson Reaction: General Procedure for the Synthesis of 8–10 and 13–16.** To a solution of the phenol-derivative (1.00 mmol) in acetone (10.0 mL), anhydrous  $K_2CO_3$  (2.2 molar equiv) and the appropriate alkyl or aryl halide (2.2 molar equiv) were added. The reaction mixture was heated to 80 °C, and reaction progress was monitored by TLC. Upon reaction completion, the mixture was hot filtered, and the solvent was evaporated under reduced pressure. The two tautomers obtained were effectively isolated from the resulting crude mixture by column chromatography over silica gel and using a mixture of PE/EtOAc as eluent. The desired final compounds were further purified by fractionated crystallization from DCM/PE. In particular, regarding the order of elution of the tautomeric mixtures, the diketone tautomer proved to elute first.

With this procedure, the following compounds were obtained.

**1E,4Z,6E-1,7-Bis-4-benzyloxyphenyl-5-hydroxyhepta-1,4,6-trien-3-one (8) and 1E,6E-1,7-Bis-4-benzyloxyphenylhepta-1,6-diene-3,5-dione (14).** Reaction of **4** (0.50 g, 1.62 mmol),  $K_2CO_3$  (0.49 g, 3.56 mmol), and benzyl bromide (0.47 mL, 3.56 mmol) gave a tautomeric mixture that was purified by flash chromatography (PE/EtOAc, 9:1). Compound **8** (Rf: 0.12) experimental characterization matched with that of the same analogue obtained by the Pabon reaction (see above). Compound **14** (Rf: 0.15): 32% yield, dark-yellow powder, mp 145–147 °C.  $^1H$  NMR (400 MHz,  $CDCl_3$ ):  $\delta$  3.96 (s, 2H,  $\beta$ -diketo- $CH_2$ ), 5.08 (s, 4H,  $OCH_2$ ), 6.87 (d, 2H,  $J = 16.0$  Hz,  $CH=CH$ ), 6.94 (d, 4H,  $J = 8.4$  Hz, Ar), 7.35–7.39 (m, 10H, Bn), 7.52 (d, 4H,  $J = 8.4$  Hz, Ar), 7.73 (d, 2H,  $J = 16.0$  Hz,  $CH=CH$ ).  $^{13}C$  NMR (101 MHz,  $CDCl_3$ ):  $\delta$  55.73, 70.44 (2C), 115.60 (4C), 122.27 (2C), 127.85 (4C), 128.40 (2C), 128.50 (2C), 129.20 (4C), 130.00 (4C), 136.91 (2C), 140.50 (2C), 160.80 (2C), 196.37 (2C). ESI-MS ( $m/z$ ): 511 ( $M + Na$ ).

**1E,4Z,6E-1,7-Bis-4-(2,4-difluorobenzyloxy)phenyl-5-hydroxyhepta-1,4,6-trien-3-one (9) and 1E,6E-1,7-Bis-4-(2,4-difluorobenzyloxy)phenylhepta-1,6-diene-3,5-dione (15).** Reaction of **4** (0.50 g, 1.60 mmol) and 2,4-difluorobenzyl bromide (0.48 mL,



3.52 mmol) gave a crude product that was purified by flash chromatography (PE/EtOAc, 9.5:0.5). Compound **9** (Rf: 0.13): yellow powder, 32% yield, 174–176 °C. <sup>1</sup>H NMR (400 MHz, CDCl<sub>3</sub>): δ 5.12 (s, 4H, OCH<sub>2</sub>), 5.79 (s, 1H, keto-enol-CH), 6.51 (d, 2H, J = 16.0 Hz, CH=CH), 6.84–6.95 (m, 4H, Ar), 6.99 (d, 4H, J = 8.4 Hz, Ar), 7.46–7.48 (m, 2H, Ar), 7.52 (d, 4H, J = 8.4 Hz, Ar), 7.61 (d, 2H, J = 16.0 Hz, CH=CH). <sup>13</sup>C NMR (101 MHz, CDCl<sub>3</sub>): δ 63.50 (2C), 104.00 (t, 2C, J = 25.6 Hz), 111.63 (dd, 2C, J = 21.4 and 3.8 Hz), 114.98 (4C), 115.17, 119.13 (dd, 2C, J = 14.6 and 4.0 Hz), 123.31, 128.48 (4C), 128.50 (2C), 130.52, 130.85 (dd, 2C, J = 9.8 and 5.3 Hz), 140.81 (2C), 160.74 (dd, 2C, J = 238.4 and 12.0 Hz), 163.23 (dd, 2C, J = 237.9 and 12.0 Hz), 163.39 (2C), 183.65 (2C). ESI-MS (*m/z*): 583 (M + Na). Compound **15** (Rf: 0.16): yellow powder, 28% yield, 153–155 °C. <sup>1</sup>H NMR (400 MHz, CDCl<sub>3</sub>): δ 3.98 (s, 2H, β-diketo-CH<sub>2</sub>), 5.11 (s, 4H, OCH<sub>2</sub>), 6.82 (d, 2H, J = 15.6 Hz, CH=CH), 6.88–6.92 (m, 4H, Ar), 6.96 (d, 4H, J = 8.4 Hz, Ar), 7.10–7.12 (m, 2H, Ar), 7.46 (d, 4H, J = 8.8 Hz, Ar), 7.75 (d, 2H, J = 15.6 Hz, CH=CH). <sup>13</sup>C NMR (101 MHz, CDCl<sub>3</sub>): δ 55.43, 63.49 (2C), 104.04 (t, 2C, J = 25.7 Hz), 111.62 (dd, 2C, J = 21.9 and 4.0 Hz), 116.37 (4C), 119.20 (dd, 2C, J = 15.1 and 4.5 Hz), 126.43 (2C), 128.59 (4C), 129.02 (2C), 130.90 (dd, 2C, J = 10.6 and 5.4 Hz), 143.07 (2C), 160.60 (dd, 2C, J = 238.7 and 12.2 Hz), 160.80 (2C), 163.03 (dd, 2C, J = 238.6 and 12.2 Hz), 196.30 (2C). ESI-MS (*m/z*): 583 (M + Na).

**1E,4Z,6E-1,7-Bis-4-(3,5-difluorobenzyloxyphenyl)-5-hydroxyhepta-1,4,6-trien-3-one (10) and 1E,6E-1,7-Bis-4-(3,5-difluorobenzyloxyphenyl)hepta-1,6-diene-3,5-dione (16).** Reaction of **4** (0.50 g, 1.60 mmol) and 3,5-difluorobenzyl bromide (0.48 mL, 3.52 mmol) gave a crude product that was purified by flash chromatography (PE/EtOAc, 9.5:0.5). Compound **10** (Rf: 0.11): 60% yield, mp 174–176 °C. <sup>1</sup>H NMR (400 MHz, CDCl<sub>3</sub>): δ 5.09 (s, 4H, OCH<sub>2</sub>), 5.80 (s, 1H, keto-enol-CH), 6.52 (d, 2H, J = 15.6 Hz, CH=CH), 6.56–6.67 (m, 2H, Ar), 6.73–6.81 (m, 2H, Ar), 6.93–6.99 (m, 2H, Ar), 6.97 (d, 4H, J = 8.8 Hz, Ar), 7.52 (d, 4H, J = 8.8 Hz, Ar), 7.63 (d, 2H, J = 15.6 Hz, CH=CH). <sup>13</sup>C NMR (101 MHz, CDCl<sub>3</sub>): δ 71.64 (2C), 102.80 (t, 2C, J = 27.7 Hz), 112.18 (dd, 4C, J = 27.3 and 4.0 Hz), 114.99, 115.14 (4C), 122.98, 128.87 (4C), 129.05, 130.10 (2C), 141.60 (t, 2C, J = 7.2 Hz), 143.81 (2C), 159.97 (2C), 164.26 (dd, 4C, J = 261.8 and 6.9 Hz), 183.50 (2C). ESI-MS (*m/z*): 583 (M + Na). Compound **16** (Rf: 0.13): yellow powder, 28% yield, mp 152–154 °C. <sup>1</sup>H NMR (400 MHz, CDCl<sub>3</sub>): δ 3.94 (s, 2H, diketo-CH<sub>2</sub>), 5.07 (s, 4H, OCH<sub>2</sub>), 6.60–6.72 (m, 2H, Ar), 6.75 (d, 2H, J = 15.2 Hz, CH=CH), 6.79–6.84 (m, 2H, Ar), 6.93 (d, 4H, J = 8.4 Hz, Ar), 6.93–6.98 (m, 2H, Ar), 7.43 (d, 4H, J = 8.8 Hz, Ar), 7.75 (d, 2H, J = 15.2 Hz, CH=CH). <sup>13</sup>C NMR (101 MHz, CDCl<sub>3</sub>): δ 55.84, 71.73 (2C), 102.98 (t, 2C, J = 27.7 Hz), 112.20 (dd, 4C, J = 27.0 and 4.0 Hz), 115.30 (4C), 127.13 (2C), 129.48 (4C), 129.50 (2C), 140.57 (t, 2C, J = 6.8 Hz), 142.41 (2C), 160.59 (2C), 164.20 (dd, 4C, J = 261.3 and 6.4 Hz) 195.06 (2C). ESI-MS (*m/z*): 583 (M + Na).

**1E,6E-1,7-Bis-4-methoxyphenylhepta-1,6-diene-3,5-dione (13).** Reaction of **4** (0.15 g, 0.49 mmol), K<sub>2</sub>CO<sub>3</sub> (0.15 g, 1.08 mmol), and iodomethane (0.07 mL, 1.08 mmol) gave the crude product that was purified by flash chromatography (PE/EtOAc, 9.5:0.5) from which **13** was obtained as the predominant component; orange-yellow powder, 44% yield, mp 103–105 °C. <sup>1</sup>H NMR (400 MHz, CDCl<sub>3</sub>): δ 3.48 (s, 2H, diketo-CH<sub>2</sub>), 3.86 (s, 6H, OCH<sub>3</sub>), 6.93 (d, 4H, J = 8.8 Hz, Ar), 7.01 (d, 2H, J = 14.8 Hz, CH=CH), 7.55 (d, 4H, J = 6.8 Hz, Ar), 7.72 (d, 2H, J = 14.8 Hz, CH=CH). <sup>13</sup>C NMR (101 MHz, CDCl<sub>3</sub>): δ 55.38 (2C), 55.43, 114.37 (4C), 121.80 (2C), 128.24 (2C), 129.75 (4C), 141.20 (2C), 161.37 (2C), 196.57 (2C). ESI-MS (*m/z*): 359 (M + Na).

**4-(4-Fluorobenzyloxy)benzaldehyde (19).** Reaction of 4-hydroxybenzaldehyde (1.24 g, 10.00 mmol) and 4-fluorobenzyl bromide (1.49 mL, 12.00 mmol) gave a crude product that was purified by flash chromatography (PE/EtOAc, 9.5:0.5); white solid, 88% yield, mp 190–192 °C. <sup>1</sup>H NMR (400 MHz, CDCl<sub>3</sub>): δ 5.08 (s, 2H, OCH<sub>2</sub>), 6.99–7.00 (m, 2H, Ar), 7.02 (d, 2H, J = 8.8 Hz, Ar), 7.10–7.14 (m, 2H, Ar), 7.82 (d, 2H, J = 8.8 Hz, Ar), 9.80 (s, 1H, CHO).

**4-(3-Fluorobenzyloxy)benzaldehyde (20).** Reaction of 4-hydroxybenzaldehyde (1.24 g, 10.00 mmol) and 3-fluorobenzyl bromide

(1.49 mL, 12.00 mmol) gave a crude product that was purified by flash chromatography (PE/EtOAc, 9.5:0.5); white solid, 85% yield, mp 183–185 °C. <sup>1</sup>H NMR (400 MHz, CDCl<sub>3</sub>): δ 5.10 (s, 2H, OCH<sub>2</sub>), 6.95 (d, 2H, J = 8.8 Hz, Ar), 6.93–6.99 (m, 1H, Ar), 7.00–7.07 (m, 2H, Ar), 7.23–7.31 (m, 1H, Ar), 7.84 (d, 2H, J = 8.8 Hz, Ar), 9.80 (s, 1H, CHO).

**Chemical Stability Studies.** The tested derivatives were dissolved in DMSO (0.50 mg/mL), and the pH of the solution was adjusted to 7.4 and 9.2 using 50 mM phosphate and 50 mM borate buffer, respectively. The obtained solutions were then maintained at room temperature and at 70 °C (oven) for 3 days and analyzed by RP-HPLC under the following conditions: the stationary phase was a phenyl-hexyl column (Xselect CSH by Waters) 4.6 × 150 mm (particle size 3.5 μm); the mobile phase was a mixture of ACN-0.1% formic acid, 70–30 (v/v) at the flow rate of 1 mL/min. The detection wavelength was 254 nm.

**BACE-1 Inhibition.** FRET inhibition studies were performed using the following procedures: 5 μL of test compound (or DMSO) were preincubated with 175 μL of BACE-1 (17.2 nM, final concentration) in 20 mM sodium acetate at pH 4.5 containing CHAPS (0.1% w/v) for 1 h at room temperature. M-2420 (3 μM, final concentration) was then added and left to react for 15 min at 37 °C. The fluorescence signal was read at λ<sub>em</sub> = 405 nm (λ<sub>exc</sub> = 320 nm). DMSO concentration in the final mixture was maintained below 5% (v/v) to guarantee no significant loss of enzyme activity. Fluorescence intensities with and without inhibitors were registered and compared. The percent inhibition due to the presence of test compounds was calculated. The background signal was measured in control wells containing all the reagents, except hrBACE-1, and subtracted. The % inhibition due to the presence of test compound was calculated by the following expression: 100 – (IF<sub>i</sub>/IF<sub>0</sub> × 100) where IF<sub>i</sub> and IF<sub>0</sub> are the fluorescence intensities obtained for hrBACE-1 in the presence and in the absence of inhibitor, respectively.<sup>43</sup> The linear regression parameters were determined and the IC<sub>50</sub> interpolated (GraphPad Prism 4.0, GraphPad Software Inc.). To demonstrate the inhibition of BACE-1 activity, a peptido-mimetic inhibitor (β-secretase inhibitor IV, Calbiochem) was serially diluted into the reactions' wells (IC<sub>50</sub> = 20 nM).

**Inhibition of GSK-3β.** Human recombinant GSK-3β was purchased from Millipore (Millipore Iberica S.A.U.). The prephosphorylated polypeptide substrate was purchased from Millipore (Millipore Iberica SAU). Kinase-Glo Luminescent Kinase Assay was obtained from Promega (Promega Biotech Iberica, SL). ATP and all other reagents were from Sigma-Aldrich (St. Louis, MO). Assay buffer contained 50 mM HEPES (pH 7.5), 1 mM EDTA, 1 mM EGTA, and 15 mM magnesium acetate. The method of Baki et al.<sup>46</sup> was followed to analyze the inhibition of GSK-3β. Kinase-Glo assays were performed in assay buffer using white 96-well plates. In a typical assay, 10 μL (10 μM) of the tested compound (dissolved in DMSO at 1 mM concentration and diluted in advance in assay buffer to the desired concentration) and 10 μL (20 ng) of enzyme were added to each well followed by 20 μL of assay buffer containing 25 μM substrate and 1 μM ATP. The final DMSO concentration in the reaction mixture did not exceed 1%. After a 30 min incubation at 30 °C, the enzymatic reaction was stopped with 40 μL of Kinase-Glo reagent. Glow-type luminescence was recorded after 10 min using a Fluoroskan Ascent multimode reader. The activity is proportional to the difference of the total and consumed ATP. The inhibitory activities were calculated on the basis of maximal kinase and luciferase activities measured in the absence of inhibitor and in the presence of a reference compound inhibitor (SB415826,<sup>65</sup> supplier, IC<sub>50</sub> = 54 nM) at total inhibition concentration, respectively. The linear regression parameters were determined and the IC<sub>50</sub> extrapolated (GraphPad Prism 4.0, GraphPad Software Inc.).

**Covalent Docking Simulation on GSK-3β.** The curcumin-optimized binding pocket from the best scoring complex of the SCARE docking procedure was used to perform a covalent docking of **5**. A thia-Michael reaction occurring between Cys199 and the α,β-unsaturated carbonyl function of **5** was simulated by means of the ICM3.7 standard covalent docking protocol.<sup>66</sup>

**Cell Culture.** The T67 human glioma cell line was derived by Lauro et al. from a World Health Organization (WHO) grade III gemistocytic astrocytoma. T67 cells were cultured in Dulbecco's modified Eagle's medium (DMEM) supplemented with 10% fetal bovine serum (FBS), 100 UI/mL penicillin, and 100  $\mu$ g/mL streptomycin in a 5% CO<sub>2</sub> atmosphere at 37 °C, with saturating humidity.

**Determination of Antioxidant Activity in T67 Cells.** To evaluate the antioxidant activity of the compounds, T67 cells were seeded in 24-well plates at  $1 \times 10^5$  cells/well. After 24 h, the cells were washed with PBS and treated for 24 h with the compounds at 10  $\mu$ M concentration. The antioxidant activity of the compounds was evaluated after 30 min of incubation with a 10  $\mu$ M fluorescent probe (2',7'-dichlorofluorescein diacetate, DCFH-DA) in DMEM, by measuring the intracellular ROS formation evoked by 30 min of exposure of T67 cells to 100  $\mu$ M *tert*-butyl hydroperoxide (TBH) in PBS. The fluorescence increase of the cells from each well was measured ( $\lambda_{exc}$  = 485 nm;  $\lambda_{em}$  = 535 nm) with a spectrofluorometer (Wallac Victor multilabel S9 counter, PerkinElmer Inc., Boston, MA). Data are reported as the mean  $\pm$  standard deviation of at least three independent experiments.

**Determination of Cell Viability (Cytotoxicity Assays).** The cytotoxicity of compounds was estimated using an MTT assay. T67 cells were seeded with complete DMEM in 24-well plates and cultured overnight. Cells were washed with PBS and incubated for 24 h at 37 °C in a humidified atmosphere, 5% CO<sub>2</sub>, with compounds at different concentrations dissolved in DMEM. After this time, cells were carefully washed with PBS and incubated for 3 h with 500  $\mu$ M thiazolyl blue tetrazolium bromide (MTT) dissolved in DMEM. Then, cells were washed with PBS and lysed with 200  $\mu$ L of dimethyl sulfoxide. The absorbance of each well was measured at 595 nm using a microplate reader (Victor2 1420 multilabel counter).

**Preparation of the Cell Homogenate.** T67 cells were treated for 24 h with 10  $\mu$ M of compounds and 2.5  $\mu$ M of 4-methylsulfinylbutyl isothiocyanate (sulforaphane) as the positive control. After this time, cells were collected and resuspended in ice-cold 50 mM potassium phosphate buffer, pH 7.4, containing 2 mM EDTA and 0.1% Triton X-100.

**Assay for NQO1 Induction.** Cellular NQO1 activity was measured according to the procedures described previously.<sup>67</sup> Briefly, the reaction mix contained 50 mM Tris-HCl, pH 7.5, 0.08% Triton X-100, 0.25 mM NADH, and 80  $\mu$ M of 2,6-dichloroindophenol (DCIP) in the presence or absence of 10  $\mu$ M dicumarol. To an assay cuvette, 0.980 mL of the reaction mix was added, and the reaction was started by adding 20  $\mu$ L of cell homogenate, and the reduction of DCIP was monitored at 600 nm, 30 °C for 3 min. The dicumarol-inhibitable NQO1 activity was calculated using the extinction coefficient of 21.0 mM<sup>-1</sup> cm<sup>-1</sup> and expressed as nmol of DCIP reduced per min/mg of cellular protein determined by the Lowry method.<sup>68</sup>

**Determination of the Chemical Stability.** Vehicle (DMSO), 5, and 13 (0.5 mg/mL) at pH 7.4 and 9.2 (adjusted with aqueous buffers) were incubated for 3 days at 70 °C (oven).

## ■ ASSOCIATED CONTENT

### ● Supporting Information

The Supporting Information is available free of charge on the ACS Publications website at DOI: 10.1021/acs.jmedchem.5b00894.

Computational studies on BACE-1 and GSK-3 $\beta$  enzymes and figures displaying the predicted binding mode of derivatives 5–8, PAMPA-BBB assay for commercial drugs, linear correlation of PAMPA-BBB assay, elemental analysis of synthesized compounds 2–16 (PDF) SMILES data (XLSX)

## ■ AUTHOR INFORMATION

### Corresponding Author

\*Phone: +39-051-2099732. Fax: +39-051-2099734. E-mail: federica.belluti@unibo.it.

### Notes

The authors declare no competing financial interest.

## ■ ACKNOWLEDGMENTS

This work was financially supported by a PRIN (20103W4779), Project Grant from MIUR, Italy. We thank Professor Roberto Gotti for performing the stability studies.

## ■ ABBREVIATIONS USED

AD, Alzheimer's disease; BACE-1,  $\beta$ -secretase; GSK-3 $\beta$ , glycogen synthase kinase-3 $\beta$ ; A $\beta$ , amyloid  $\beta$ ; SPs, senile plaques; NFTs, neurofibrillary tangles; APP, amyloid  $\beta$  protein precursor; NQO1, NAD(P)H:quinone oxidoreductase 1; CNS, central nervous system; ROS, reactive oxygen species; BBB, blood–brain barrier; FRET, fluorescence resonance energy transfer; ADME, absorption, distribution, metabolism, excretion; PAMPA, parallel artificial membrane permeability assay; TBH, *tert*-butyl hydroperoxide

## ■ REFERENCES

- (1) Dulsat, C. A report from the 65th Annual Meeting of the American Academy of Neurology (March 16–23, 2013, San Diego, California, USA). *Drugs Today (Barc)* **2013**, 49 (5), 341–5.
- (2) Cummings, J. L. Treatment of Alzheimer's disease: current and future therapeutic approaches. *Rev. Neurol. Dis.* **2004**, 1 (2), 60–69.
- (3) Lazarov, O.; Marr, R. A. Neurogenesis and Alzheimer's disease: at the crossroads. *Exp. Neurol.* **2010**, 223 (2), 267–281.
- (4) Marx, J. A New Take on Tau. *Science* **2007**, 316 (5830), 1416–1417.
- (5) Walsh, D. M.; Selkoe, D. J. Deciphering the molecular basis of memory failure in Alzheimer's disease. *Neuron* **2004**, 44 (1), 181–193.
- (6) Schneider, L. S.; Mangialasche, F.; Andreasen, N.; Feldman, H.; Giacobini, E.; Jones, R.; Mantua, V.; Mecocci, P.; Pani, L.; Winblad, B.; Kivipelto, M. Clinical trials and late-stage drug development for Alzheimer's disease: an appraisal from 1984 to 2014. *J. Intern. Med.* **2014**, 275 (3), 251–283.
- (7) Golde, T. E.; Eckman, C. B.; Younkin, S. G. Biochemical detection of Abeta isoforms: implications for pathogenesis, diagnosis, and treatment of Alzheimer's disease. *Biochim. Biophys. Acta, Mol. Basis Dis.* **2000**, 1502 (1), 172–187.
- (8) Golde, T. E. Alzheimer disease therapy: can the amyloid cascade be halted? *J. Clin. Invest.* **2003**, 111 (1), 11–18.
- (9) Tamagno, E.; Bardini, P.; Obbili, A.; Vitali, A.; Borghi, R.; Zaccheo, D.; Pronzato, M. A.; Danni, O.; Smith, M. A.; Perry, G.; Tabaton, M. Oxidative stress increases expression and activity of BACE in NT2 neurons. *Neurobiol. Dis.* **2002**, 10 (3), 279–288.
- (10) Ghosh, A. K.; Gemma, S.; Tang, J. beta-secretase as a therapeutic target for Alzheimer's disease. *Neurotherapeutics* **2008**, 5 (3), 399–408.
- (11) Ittner, L. M.; Götz, J. Amyloid- $\beta$  and tau—a toxic pas de deux in Alzheimer's disease. *Nat. Rev. Neurosci.* **2011**, 12 (2), 65–72.
- (12) Weingarten, M. D.; Lockwood, A. H.; Hwo, S. Y.; Kirschner, M. W. A protein factor essential for microtubule assembly. *Proc. Natl. Acad. Sci. U. S. A.* **1975**, 72 (5), 1858–1862.
- (13) Avila, J. Tau phosphorylation and aggregation in Alzheimer's disease pathology. *FEBS Lett.* **2006**, 580 (12), 2922–2927.
- (14) Llorens-Martín, M.; Jurado, J.; Hernández, F.; Avila, J. GSK-3 $\beta$ , a pivotal kinase in Alzheimer disease. *Front. Mol. Neurosci.* **2014**, 7, 46.
- (15) Billingsley, M. L.; Kincaid, R. L. Regulated phosphorylation and dephosphorylation of tau protein: effects on microtubule interaction, intracellular trafficking and neurodegeneration. *Biochem. J.* **1997**, 323 (Pt 3), 577–591.



- (16) Martinez, A.; Perez, D. I.; Gil, C. Lessons learnt from glycogen synthase kinase 3 inhibitors development for Alzheimer's disease. *Curr. Top. Med. Chem.* **2013**, *13* (15), 1808–1819.
- (17) Perez, D. I.; Conde, S.; Perez, C.; Gil, C.; Simon, D.; Wandosell, F.; Moreno, F. J.; Gelpi, J. L.; Luque, F. J.; Martinez, A. Thienylhalomethylketones: Irreversible glycogen synthase kinase 3 inhibitors as useful pharmacological tools. *Bioorg. Med. Chem.* **2009**, *17* (19), 6914–6925. Perez, D. I.; Palomo, V.; Perez, C.; Gil, C.; Dans, P. D.; Luque, F. J.; Conde, S.; Martinez, A. Switching Reversibility to Irreversibility in Glycogen Synthase Kinase 3 Inhibitors: Clues for Specific Design of New Compounds. *J. Med. Chem.* **2011**, *54* (12), 4042–4056.
- (18) Perez, D. I.; Palomo, V.; Perez, C.; Gil, C.; Dans, P. D.; Luque, F. J.; Conde, S.; Martinez, A. Switching Reversibility to Irreversibility in Glycogen Synthase Kinase 3 Inhibitors: Clues for Specific Design of New Compounds. *J. Med. Chem.* **2011**, *54* (12), 4042–4056.
- (19) Busciglio, J.; Lorenzo, A.; Yeh, J.; Yankner, B. A. beta-amyloid fibrils induce tau phosphorylation and loss of microtubule binding. *Neuron* **1995**, *14* (4), 879–888.
- (20) Zheng, W. H.; Bastianetto, S.; Mennicken, F.; Ma, W.; Kar, S. Amyloid beta peptide induces tau phosphorylation and loss of cholinergic neurons in rat primary septal cultures. *Neuroscience* **2002**, *115* (1), 201–211.
- (21) Golde, T. E. Disease modifying therapy for AD? *J. Neurochem.* **2006**, *99* (3), 689–707.
- (22) Grill, J. D.; Cummings, J. L. Current therapeutic targets for the treatment of Alzheimer's disease. *Expert Rev. Neurother.* **2010**, *10* (5), 711–728.
- (23) Cavalli, A.; Bolognesi, M. L.; Minarini, A.; Rosini, M.; Tumiatti, V.; Recanatini, M.; Melchiorre, C. Multi-target-directed ligands to combat neurodegenerative diseases. *J. Med. Chem.* **2008**, *51* (3), 347–72.
- (24) Viayna, E.; Sola, I.; Di Pietro, O.; Muñoz-Torrero, D. Human disease and drug pharmacology, complex as real life. *Curr. Med. Chem.* **2013**, *20* (13), 1623–1634.
- (25) Zheng, H.; Fridkin, M.; Youdim, M. From single target to multitarget/network therapeutics in Alzheimer's therapy. *Pharmaceuticals* **2014**, *7* (2), 113–135.
- (26) Morphy, R.; Kay, C.; Rankovic, Z. From magic bullets to designed multiple ligands. *Drug Discovery Today* **2004**, *9* (15), 641–651.
- (27) Prati, F.; De Simone, A.; Bisignano, P.; Armirotti, A.; Summa, M.; Pizzirani, D.; Scarpelli, R.; Perez, D. I.; Andrisano, V.; Perez-Castillo, A.; Monti, B.; Massenzio, F.; Polito, L.; Racchi, M.; Favia, A. D.; Bottegoni, G.; Martinez, A.; Bolognesi, M. L.; Cavalli, A. Multitarget drug discovery for Alzheimer's disease: triazinones as BACE-1 and GSK-3 $\beta$  inhibitors. *Angew. Chem., Int. Ed.* **2015**, *54* (5), 1578–1582.
- (28) Belluti, F.; De Simone, A.; Tarozzi, A.; Bartolini, M.; Djemil, A.; Bisi, A.; Gobbi, S.; Montanari, S.; Cavalli, A.; Andrisano, V.; Bottegoni, G.; Rampa, A. Fluorinated benzophenone derivatives: balanced multipotent agents for Alzheimer's disease. *Eur. J. Med. Chem.* **2014**, *78*, 157–166.
- (29) Rizzo, S.; Tarozzi, A.; Bartolini, M.; Da Costa, G.; Bisi, A.; Gobbi, S.; Belluti, F.; Ligresti, A.; Allara, M.; Monti, J. P.; Andrisano, V.; Di Marzo, V.; Hrelia, P.; Rampa, A. 2-Arylbenzofuran-based molecules as multipotent Alzheimer's disease modifying agents. *Eur. J. Med. Chem.* **2012**, *58*, 519–532.
- (30) Newman, D. J.; Cragg, G. M.; Snader, K. M. Natural products as sources of new drugs over the period 1981–2002. *J. Nat. Prod.* **2003**, *66* (7), 1022–1037.
- (31) Evans, B. E.; Rittle, K. E.; Bock, M. G.; DiPardo, R. M.; Freidinger, R. M.; Whitter, W. L.; Lundell, G. F.; Veber, D. F.; Anderson, P. S. Methods for drug discovery: development of potent, selective, orally effective cholecystokinin antagonists. *J. Med. Chem.* **1988**, *31* (12), 2235–2246.
- (32) Aggarwal, B. B.; Sundaram, C.; Malani, N.; Ichikawa, H. Curcumin: the Indian solid gold. *Adv. Exp. Med. Biol.* **2007**, *595*, 1–75.
- (33) Prasad, S.; Gupta, S. C.; Tyagi, A. K.; Aggarwal, B. B. Curcumin, a component of golden spice: from bedside to bench and back. *Biotechnol. Adv.* **2014**, *32* (6), 1053–1064.
- (34) Anand, P.; Thomas, S. G.; Kunnumakkara, A. B.; Sundaram, C.; Harikumar, K. B.; Sung, B.; Tharakan, S. T.; Misra, K.; Priyadarsini, I. K.; Rajasekharan, K. N.; Aggarwal, B. B. Biological activities of curcumin and its analogues (Congeners) made by man and Mother Nature. *Biochem. Pharmacol.* **2008**, *76* (11), 1590–1611.
- (35) Chin, D.; Huebbe, P.; Pallauf, K.; Rimbach, G. Neuroprotective Properties of Curcumin in Alzheimer's Disease - Merits and Limitations. *Curr. Med. Chem.* **2013**, *20* (32), 3955–3985.
- (36) Esatbeyoglu, T.; Huebbe, P.; Ernst, I. M.; Chin, D.; Wagner, A. E.; Rimbach, G. Curcumin—from molecule to biological function. *Angew. Chem., Int. Ed.* **2012**, *51* (22), S308–S332.
- (37) Payton, F.; Sandusky, P.; Alworth, W. L. NMR study of the solution structure of curcumin. *J. Nat. Prod.* **2007**, *70* (2), 143–146.
- (38) Benassi, R.; Ferrari, E.; Lazzari, S.; Spagnolo, F.; Saladini, M. Theoretical study on Curcumin: A comparison of calculated spectroscopic properties with NMR, UV-vis and IR experimental data. *J. Mol. Struct.* **2008**, *892* (1–3), 168–176.
- (39) Amslinger, S. The tunable functionality of alpha,beta-unsaturated carbonyl compounds enables their differential application in biological systems. *ChemMedChem* **2010**, *5* (3), 351–356.
- (40) Bustanji, Y.; Taha, M. O.; Almasri, I. M.; Al-Ghussein, M. A.; Mohammad, M. K.; Alkhatib, H. S. Inhibition of glycogen synthase kinase by curcumin: Investigation by simulated molecular docking and subsequent in vitro/in vivo evaluation. *J. Enz. Inhib. Med. Chem.* **2009**, *24* (3), 771–778.
- (41) Wang, X.; Kim, J. R.; Lee, S. B.; Kim, Y. J.; Jung, M. Y.; Kwon, H. W.; Ahn, Y. J. Effects of curcuminoids identified in rhizomes of *Curcuma longa* on BACE-1 inhibitory and behavioral activity and lifespan of Alzheimer's disease *Drosophila* models. *BMC Complementary Altern. Med.* **2014**, *14*, 88.
- (42) Pabon, H. J. A synthesis of curcumin and related compounds. *Recl. Trav. Chim. Pays-Bas* **1964**, *83*, 379–386.
- (43) Mancini, F.; De Simone, A.; Andrisano, V. Beta-secretase as a target for Alzheimer's disease drug discovery: an overview of in vitro methods for characterization of inhibitors. *Anal. Bioanal. Chem.* **2011**, *400* (7), 1979–1996.
- (44) Hagmann, W. K. The many roles for fluorine in medicinal chemistry. *J. Med. Chem.* **2008**, *51* (15), 4359–4369.
- (45) Silvestri, R. Boom in the development of non-peptidic beta-secretase (BACE1) inhibitors for the treatment of Alzheimer's disease. *Med. Res. Rev.* **2009**, *29* (2), 295–338.
- (46) Baki, A.; Bielak, A.; Molnár, L.; Szendrei, G.; Keserü, G. M. A high throughput luminescent assay for glycogen synthase kinase-3beta inhibitors. *Assay Drug Dev. Technol.* **2007**, *5* (1), 75–83.
- (47) London, N.; Miller, R. M.; Krishnan, S.; Uchida, K.; Irwin, J. J.; Eidam, O.; Gibold, L.; Cimermančič, P.; Bonnet, R.; Schoichet, B. K.; Taunton, J. Covalent docking of large libraries for the discovery of chemical probes. *Nat. Chem. Biol.* **2014**, *10* (12), 1066–1072.
- (48) Minassi, A.; Sánchez-Duffhues, G.; Collado, J. A.; Muñoz, E.; Appendino, G. Dissecting the pharmacophore of curcumin. Which structural element is critical for which action? *J. Nat. Prod.* **2013**, *76* (6), 1105–1112.
- (49) Avonto, C.; Taglialatela-Scafati, O.; Pollastro, F.; Minassi, A.; Di Marzo, V.; De Petrocellis, L.; Appendino, G. An NMR spectroscopic method to identify and classify thiol-trapping agents: revival of Michael acceptors for drug discovery? *Angew. Chem., Int. Ed.* **2011**, *50* (2), 467–471.
- (50) Wang, Y. J.; Pan, M. H.; Cheng, A. L.; Lin, L. I.; Ho, Y. S.; Hsieh, C. Y.; Lin, J. K. Stability of curcumin in buffer solutions and characterization of its degradation products. *J. Pharm. Biomed. Anal.* **1997**, *15* (12), 1867–1876.
- (51) Dahmke, I. N.; Boettcher, S. P.; Groh, M.; Mahlknecht, U. Cooking enhances curcumin anti-carcinogenic activity through pyrolytic formation of "deketene curcumin". *Food Chem.* **2014**, *151*, 514–519.

- (52) Cardoso, F. L.; Brites, D.; Brito, M. A. Looking at the blood-brain barrier: molecular anatomy and possible investigation approaches. *Brain Res. Rev.* **2010**, *64* (2), 328–363.
- (53) van Asperen, J.; Mayer, U.; van Tellingen, O.; Beijnen, J. H. The functional role of P-glycoprotein in the blood-brain barrier. *J. Pharm. Sci.* **1997**, *86* (8), 881–884.
- (54) Begum, A. N.; Jones, M. R.; Lim, G. P.; Morihara, T.; Kim, P.; Heath, D. D.; Rock, C. L.; Pruitt, M. A.; Yang, F.; Hudspeth, B.; Hu, S.; Faull, K. F.; Teter, B.; Cole, G. M.; Frautschy, S. A. Curcumin structure-function, bioavailability, and efficacy in models of neuro-inflammation and Alzheimer's disease. *J. Pharmacol. Exp. Ther.* **2008**, *326* (1), 196–208.
- (55) Di, L.; Kerns, E. H.; Fan, K.; McConnell, O. J.; Carter, G. T. High throughput artificial membrane permeability assay for blood-brain barrier. *Eur. J. Med. Chem.* **2003**, *38* (3), 223–232.
- (56) Crivori, P.; Cruciani, G.; Carrupt, P. A.; Testa, B. Predicting blood-brain barrier permeation from three-dimensional molecular structure. *J. Med. Chem.* **2000**, *43* (11), 2204–2216.
- (57) Zhu, X.; Su, B.; Wang, X.; Smith, M. A.; Perry, G. Causes of oxidative stress in Alzheimer disease. *Cell. Mol. Life Sci.* **2007**, *64* (17), 2202–2210.
- (58) Siegel, D.; Gustafson, D. L.; Dehn, D. L.; Han, J. Y.; Boonchoong, P.; Berliner, L. J.; Ross, D. NAD(P)H:quinone oxidoreductase 1: role as a superoxide scavenger. *Mol. Pharmacol.* **2004**, *65* (5), 1238–1247.
- (59) Torres-Lista, V.; Parrado-Fernández, C.; Alvarez-Montón, I.; Frontiñán-Rubio, J.; Durán-Prado, M.; Peinado, J. R.; Johansson, B.; Alcaín, F. J.; Giménez-Llort, L. Neophobia, NQO1 and SIRT1 as premorbid and prodromal indicators of AD in 3xTg-AD mice. *Behav. Brain Res.* **2014**, *271*, 140–146.
- (60) Tsvetkov, P.; Asher, G.; Reiss, V.; Shaul, Y.; Sachs, L.; Lotern, J. Inhibition of NAD(P)H: quinone oxidoreductase 1 activity and induction of p53 degradation by the natural phenolic compound curcumin. *Proc. Natl. Acad. Sci. U. S. A.* **2005**, *102* (15), 5535–5540.
- (61) Capurro, V.; Busquet, P.; Lopes, J. P.; Bertorelli, R.; Tarozzo, G.; Bolognesi, M. L.; Piomelli, D.; Reggiani, A.; Cavalli, A. Pharmacological characterization of memoquin, a multi-target compound for the treatment of Alzheimer's disease. *PLoS One* **2013**, *8* (2), e56870.
- (62) Manson, M. M. Inhibition of survival signalling by dietary polyphenols and indole-3-carbinol. *Eur. J. Cancer* **2005**, *41* (13), 1842–1853.
- (63) Lin, L.; Shi, Q.; Nyarko, A. K.; Bastow, K. F.; Wu, C. C.; Su, C. Y.; Shih, C. C.; Lee, K. H. Antitumor agents. 250. Design and synthesis of new curcumin analogues as potential anti-prostate cancer agents. *J. Med. Chem.* **2006**, *49* (13), 3963–3972.
- (64) Saladini, M.; Lazzari, S.; Pignedoli, F.; Rosa, R.; Spagnolo, F.; Ferrari, E. New synthetic glucosyl-curcuminoids, and their <sup>1</sup>H and <sup>13</sup>C NMR characterization, from *Curcuma longa* L. *Plant Foods Hum. Nutr.* **2009**, *64* (3), 224–229.
- (65) Coghlan, M. P.; Culbert, A. A.; Cross, D. A.; Corcoran, S. L.; Yates, J. W.; Pearce, N. J.; Rausch, O. L.; Murphy, G. J.; Carter, P. S.; Roxbee Cox, L.; Mills, D.; Brown, M. J.; Haigh, D.; Ward, R. W.; Smith, D. G.; Murray, K. J.; Reith, A. D.; Holder, J. C. Selective small molecule inhibitors of glycogen synthase kinase-3 modulate glycogen metabolism and gene transcription. *Chem. Biol.* **2000**, *7* (10), 793–803.
- (66) Abagyan, R.; Raush, E.; Totrov, M. ICM Manual v.3.7. <http://www.molsoft.com/man/index.html>.
- (67) Jia, Z.; Zhu, H.; Misra, H. P.; Li, Y. Potent induction of total cellular GSH and NQO1 as well as mitochondrial GSH by 3H-1,2-dithiole-3-thione in SH-SY5Y neuroblastoma cells and primary human neurons: protection against neurocytotoxicity elicited by dopamine, 6-hydroxydopamine, 4-hydroxy-2-nonenal, or hydrogen peroxide. *Brain Res.* **2008**, *1197*, 159–169.
- (68) Lowry, O. H.; Rosebrough, N. J.; Farr, A. L.; Randall, R. J. Protein measurement with the Folin phenol reagent. *J. Biol. Chem.* **1951**, *193* (1), 265–275.